2013

Thermophysical properties study of micro/nano materials

Guoqing Liu
Iowa State University

Thermophysical properties study of micro/nano materials

by

Guoqing Liu

A dissertation submitted to the graduate faculty

in partial fulfillment of the requirements for the degree of

DOCTOR OF PHILOSOPHY

Major: Mechanical Engineering

Program of Study Committee:
Xinwei Wang, Major Professor
Chenxu Yu
Wei Hong
Gap-Yong Kim
Terry Meyer

Iowa State University

Ames, Iowa

2013

TABLE OF CONTENTS

LIST OF FIGURES

Page

LIST OF TABLES

Page

ACKNOWLEDGEMENTS

I would like to thank my major advisor, Professor Xinwei Wang, without his amazing mentorship and continuous support, this work would not have been possible. I would also like to thank my committee members, Professor Chenxu Yu, Professor Wei Hong, Professor Gap-Yong Kim, and Professor Terry Meyer, for their great guidance throughout the course of this research.

Support of this work from Office of Naval Research (N000141210603) and the Army Research Office (W911NF1010381) is gratefully acknowledged. Partial support of this work from the National Science Foundation (CBET-0931290, CMMI-0926704, and CBET-0932573) is also acknowledged.

Studying at Iowa State University is always a wonderful experience. Last year, when I was asked by a prospective student, what's my opinion about Iowa State, I said that, you can go anywhere from here.

Finally, thanks to my girlfriend and parents for their love and encouragement.

ABSTRACT

Thermal transport in micro/nano materials is very critical, not only because the thermal property may have important influence on the performance of the materials, but also because the change of this property can reflect the inner structure change. Due to the complicated structure and small scale, the thermal properties of biomaterials, such as silkworm silk, spider silk and human head hair, are still not fully understood.

Experiments are conducted on silkworm silk, spider silk and human head hair to explore their thermal properties and potential applications. This work reports on the first time study of thermal transport in the axial direction of single silkworm silks. The measured thermal diffusivity of relaxed silkworm silk and thermal conductivity are 0.39 $\times 10^{-6}$~2.03 $\times 10^{-6}$ m^2 s^{-1} and 0.54~6.53 W m^{-1} K^{-1}, respectively. The thermal diffusivity of silkworm silk increases up to 263% upon elongation up to 63.8%. For one of the samples studied (sample 5), its thermal conductivity goes up to 13.1 W m^{-1} K^{-1} after elongation of 68.3%, surpassing many other polymers. Three factors combine together to give rise of the remarkable thermal diffusivity increase: alignment improvement of β-sheets blocks, straightening of α-helices and random coils under stretching, and structural transformation from α-helices and random coils to β-sheets crystal by elongation (confirmed by our Raman spectroscopy study). Thermal path break-down is observed when elongation is beyond 63.8%. Our Raman spectroscopy study confirms

this speculation: after 60% elongation, the Raman frequency started to increase, indicating the internal stress has been released due to internal structure break-down.

Through series of experiments, a linear relationship between the effective thermal diffusivity and pressure-which has an effect on the effective thermal diffusivity in the form of gas conduction-is discovered and proved. By testing samples with different length, the effect of radiation and gas conduction can be eliminated. In the second part, this work reports on the much more accurate characterization of thermal transport in the axial direction of single silkworm silk, spider silk and human head hair (three parts: at the root, in the middle, and at the tip). The measured real thermal diffusivity of silkworm silk, spider silk and human head hair is 3.68×10^{-7} m^2 s^{-1}, 3.53×10^{-7} m^2 s^{-1}, 1.53×10^{-7} m^2 s^{-1} (at the root), 1.40×10^{-7} m^2 s^{-1} (in the middle) and 1.49×10^{-7} m^2 s^{-1} (at the tip), respectively. The thermal conductivity and effective emissivity of the materials can also be calculated with the given value of volume-based specific heat (ρc_p).

After characterizing the original samples, the study of thermal transport in the axial direction of single filaments of silk (*Bombyx mori*) fibroin before and after heat treatment is performed. The measured thermal diffusivity of the original silk fibroin fiber ranges from 4.05×10^{-7} to 4.65×10^{-7} m^2 s^{-1}. After heat treatment (from about 140 °C to about 220 °C) and subtracting the gold and radiation effect, the real thermal diffusivity

of silk fibroin type 1, 2 and 3, increase by 38.12%, 20.72% and 21.35%, respectively. The sample diameter change is almost negligible which is proved by checking the diameter of the sample at the same place before and after heat treatment by SEM. Raman analysis was performed on the original and heat-treated (heated at about 147 °C and 179 °C) samples. After the heat treatment at 147 °C, the peaks at 1081, 1230 and 1665 cm^{-1} become slightly sharper, which is a probable sign of structural transformation from amorphous region to crystalline region. According to the literature, a model composed of amorphous regions, crystalline regions and laterally ordered regions is proposed to explain the structural changes induced by heat treatment. Due to the close packing of the more adjacent laterally ordered regions, the number and size of the crystalline regions of *Bombyx mori* silk fibroin increased by heat treatment. Thus the thermal properties of the samples are significantly improved.

CHAPTER 1. INTRODUCTION

1.1 Thermal transport in one-dimensional structures: biomaterials (fibers)

In the past, very limited effort has been reported on the thermal transport in protein fibers, such as silkworm silk, spider silk and human head hair. The thermal transport properties, like thermal conductivity and thermal diffusivity, are highly related to the protein's molecular weight, crystallinity, alignment, defects, and secondary structure. So the thermal transport properties can be very important parameters (signature) to reflect the overall structure of the proteins in the fibers. On one hand, protein fibers can be treated as special polymer materials.

In these organic materials (silkworm silk, spider silk and human head hair) mentioned above, silkworm silk fiber is special. It is a fibrous protein composed of two strands of fibroin coated with a layer of sericin. It is widely used and has a lot of advantages like comfort, high mechanical strength and elasticity [1]. In the past century, this material also provided important clinical repair options for many applications, such as biomaterial suture material [2]. With the development of biomedical and biotechnological engineering, it finds more and more applications in these fields, such as biosensors, drug delivery, etc [2-5]. The silkworm silk fibroin fibers are about 10-25 μm in diameter. The existing research about the silkworm silk is mainly focused on the protein structure [6-8], mechanical properties and genetics from the point view of

biology [9, 10]. Many theoretical models have been developed to relate the properties of silkworm silks to their structures [11, 12]. Until now the thermal conductivity along the axial direction of silkworm silk has never been reported, largely due to the great difficulty imposed by the small fiber size on measurement. Relative work done before is about the silk-cloth's thermal conductivity in the thickness-direction [13]. The reported value is about 0.042 W/m·K. Because of the contact resistance and porosity among silkworm silk fibers in silk-cloth, the reported thermal conductivity is an effective value of the silk-cloth. According to the silk-cloth producing method, this effective value is largely determined by the radial thermal conductivity of silk. It does not reflect the axial thermal transport capacity of single silkworm silk fibers.

Based on the preparation method, there are two types of silkworm silk: original (not degummed) samples and degummed samples. When this material is used as suture, the sericin needs to be removed from the silk fibroin fibers, and the fibroin fibers will be coated with waxes or silicone to reduce fraying [2]. Recent study [2] shows that the residual sericin may cause some biocompatibility problems, for example, allergic response. So it is very critical that, in order to avoid the similar problems caused by the sericin in the future, the properties of degummed silk (fibroin) fibers need to be fully characterized and recognized, and the thermal property is one of the most important properties.

Different researches have been conducted on the thermal transport in polymer materials. There are three important aspects to interpret the thermal conductivity of polymers: the temperature dependence, the crystallinity dependence and the orientation effect [14]. The thermal conductivity for all amorphous polymers is approximately equal in magnitude and characterized by a T^2 (T: temperature) dependence below 0.5 K, a plateau region between 5 and 15 K and a slow increase at higher temperatures. The thermal conductivity of semicrystalline polymers shows both strong crystallinity and temperature dependence, with a distinctive cross-over point at about 10 K. Orientation causes very large anisotropy in semicrystalline polymers, which however decreases at low temperature and becomes insignificant below 10 K [14]. In order to enhance the electrical and thermal conductivity of polymers, many other materials are filled into polymers. The hybrid filler, which consists of spherical and fibrous filler, can enhance the thermal conductivity of polymer composites at low to intermediate filler content [15]. Metals are also good fillers to improve the thermal conductivity of polymers. When the filler (aluminum powder) content is low, 0-12% by volume, the particles are distributed homogeneously in the polymer matrix and have no interaction with each other. At higher particle content, the filler will form agglomerates and conductive chains will result in a rapid increase in thermal conductivity [16].

Special treatment of the materials, such as stretching, heat treatment, and temperature-controlled water vapor annealing, can also change the thermal properties of

the materials. For organic materials, research has offered clear evidence that the thermal conductivity along the direction of molecular orientation will be improved by tensile strain [17-19]. For instance, the thermal conductivity (parallel to the stretching direction) of single crystal mat polyethylene was increased to 41.8 W m^{-1} K^{-1} when the draw ratio is 350 while the thermal conductivity of melt-crystallized polyethylene is about 3 W m^{-1} K^{-1} before stretching. The effect of stretching on the axial and transverse thermal conductivity of polyethylene is different. The axial thermal conductivity is improved as draw ratio increases, and for transverse thermal conductivity, it is negatively influenced [20]. The anisotropy of thermal conductivity is also observed in linear amorphous high polymers, and the change tendency of the axial and transverse thermal conductivity caused by stretching is the same as that of single crystal mat polyethylene [21]. A network theory for the thermal conductivity of amorphous polymeric material has been proposed [22]. In that study, the thermal conductivity of polymer was increased by about 100% when the elongation is 100%. This provides a promising way to improve organic material's thermal conductivity and diffusivity. Thermally induced crystallization is another interesting phenomenon, which is found in many materials, such as amorphous $Ge_{0.4}$ $Se_{0.6}$ [23] and titania films [24]. For reconstituted silk fibroin (RSF) films, the original film is completely noncrystalline prior to the treatment. When heated above the glass transition temperature (T_g), the crystallinity can increase to 43% at 214 °C [3]. For this same material, when treated by temperature-controlled water vapor annealing, the β-sheets crystallinity can increase from 14% (when the water vapor annealing temperature

is 4 °C) to 57.8-59.6% (when the water vapor annealing temperature is 90-100 °C) [25].

Due to the fact that the single filament of protein fibers is only μm thickness, very little research about the thermal transport in these materials has been conducted. Many attempts have been tried to measure the thermal properties in protein fibers in our lab, such as spider silk [26] and silkworm silk [27]. The experiment results show that the thermal conductivity of silkworm silk is only 0.54–6.53 W $m^{-1} K^{-1}$, but spider silk has exceptionally high thermal conductivity, which is almost close to that of the second best metallic conductor: copper. Both of these two materials show abnormal thermal transport change (improvement) under stretching. For spider silk, the measured thermal diffusivity α varies from 8.38 ± 0.81 × 10^{-5} to 12.30 ± 1.18 × 10^{-5} m^2 s^{-1} (46.8% increase) and thermal conductivity k is from 348.7 ± 33.4 to 415.9 ± 33.0 W $m^{-1} K^{-1}$ (19.3% increase) under strain from 3.9% to 19.7%, respectively. The thermal diffusivity of silkworm silk increases by up to 263% upon elongation up to 63.8%. For one of the samples studied, the thermal conductivity goes up to 13.1 W $m^{-1} K^{-1}$ after elongation of 68.3%, surpassing many other polymers. The work mentioned above is a very complicated one that involves surface radiation effect, surface roughness, and gas conduction effect in the vacuum chamber used in the experiment. Also the very thin thickness of the samples has placed great difficulty on the measurement.

In the past, the single wire 3ω method [28-30] and the micro-fabricated device

method [31-35] have been developed to measure the thermal properties of one dimensional structures at the micro/nanoscale. A technique based on optical heating and electrical thermal sensing (OHETS) has been developed to characterize the thermal properties of human head hair [36]. Two samples, one is 2.718 mm long, and the other one is 4.013 mm, have been characterized by this technique. The thermal diffusivity of these two samples is 1.94×10^{-6} $m^2 s^{-1}$ and 4.13×10^{-6} $m^2 s^{-1}$, respectively. In order to broaden the measurement scope of materials (conductive and nonconductive) and improve the accuracy and stability, we have developed the transient electro-thermal technique (TET) for characterization of thermophysical properties of micro/nanoscale wires. The TET has been applied to characterize the thermal properties of free-standing micrometer-thick Poly (3-hexylthiophene) films [37], thin films composed of anatase TiO_2 nanofibers [38], single-wall carbon nanotubes [39], and micro/sub-microscale polyacrylonitrile wires [40].

Then we noticed that, the less accurate experimental control may decrease the accuracy of the experimental data. Also the radiation effect is not precisely subtracted from the measurement. This effect could be very important especially for long samples in the measurement and samples of low thermal conductivity. So based on TET, a new method and procedure are developed to subtract the effect of radiation and gas conduction by only testing two samples with different length.

1.2 Scope of present work

After the sample is prepared, TET and calibration are combined to characterize the thermal properties (thermal diffusivity α, thermal conductivity k, and volume-based specific heat ρc_p) of the sample. Based on TET, a new method and procedure to subtract the effect of radiation and gas conduction by only testing two samples with different length are developed, tested and applied. Other than thermal properties, other physical properties such as inner structures are also our interest with specific materials. In Chapter 2, the theoretical principals and background of TET, calibration and the new technique are introduced. In Chapter 3, silkworm silks are hand reeled from cocoons and characterized for their thermal transport capacity under relaxed and stretched conditions. A structural model is established to explain the observed improvement of the thermal diffusivity and thermal path breakdown. Raman analysis is performed to study the structure change of the silkworm silk under large elongation, in anticipation to understand the physics behind the thermal diffusivity increase. In Chapter 4, a theory is developed to consider the effect of surface radiation and gas conduction during thermal characterization of one-dimensional protein fibers. The gas conduction effect and radiation effect is precisely subtracted by studying the measured thermal diffusivity variation under different pressure and samples (silkworm silk, spider silk and human head hair) of different lengths. By using available volume-based specific heat (ρc_p) of samples, the real thermal conductivity and surface emissivity of these protein fibers can also be evaluated. In Chapter 5, the effect of heat treatment on the thermal properties of

three types of degummed silkworm silk fibroin fibers is evaluated. Raman analysis is also applied to check the structural change of the samples, and a model is proposed to explain the improvement of thermal properties.

CHAPTER 2. THERMAL CHARACTERIZATION PRINCIPLES AND TECHNIQUES

In this chapter, the transient electrothermal (TET) technique and calibration are introduced in detail. The thermal properties which can be characterized by the combination of these two techniques are thermal diffusivity α, thermal conductivity k, and volume-based specific heat ρc_p. The thermal diffusivity is directly determined by curve fitting (TET technique); the thermal conductivity can be calculated after the temperature coefficient of resistance ($\eta = \Delta R/\Delta T$) is got by calibration. Because $\rho c_p = k/\alpha$, so the volume-based specific heat can also be calculated. In order to eliminate the effect of radiation and gas conduction, a new technique is developed based on TET, which is used to accurately characterize the thermal properties of silkworm silks, spider silks and human head hair.

2.1 Transient electrothermal (TET) technique

2.1.1 Experimental configuration

In TET technique, the sample is suspended between two copper electrodes (Fig. 2-1). Silver paste is used to enhance electrical conduction. For biomaterials, because they are nonconductive, a gold film (~nm) is coated on the sample surface to make it electrically conductive. In order to reduce the air convection effect, the sample is placed in a vacuum chamber and the pressure will be pumped down to about 1 mTorr. A current

source is used to provide constant current and introduce electrical heating. Upon this step current joule heating, the sample will experience a quick temperature increase. The schematic induced voltage-time (*V*-*t*) profile recorded by the oscilloscope is shown in Fig. 2-2. How fast/slow the temperature increases is determined by two competing processes: one is the joule heating, and the other one is the heat conduction from the sample to the electrodes. A higher thermal diffusivity of the sample will lead to a faster temperature evolution, meaning a shorter time to reach the steady state. Therefore, the transient voltage/temperature change can be used to determine the thermal diffusivity. When determining thermal diffusivity of the sample, no real temperature rise is needed. In fact, only the normalized temperature rise based on the voltage increase is used.

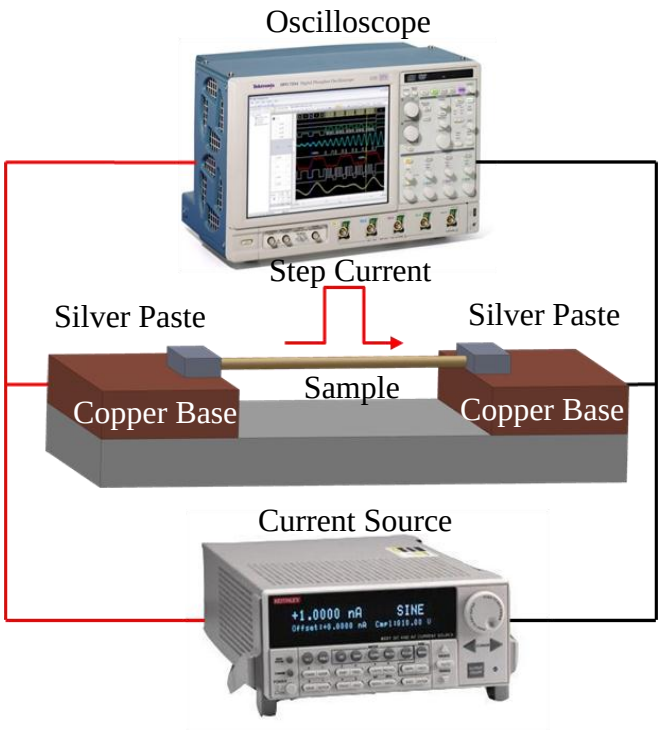

Figure 2-1. Experimental configuration of transient electrothermal (TET) technique.

2.1.2 Theoretical principles

For the biomaterials tested in this work, the diameter is very small when it is compared to the sample length (~mm). For example, the diameter for spider silk is only about 2 μm, for silkworm silk, it is about 10-20 μm, and for human head hair, it is about 80 μm. Therefore the heat transfer along the x direction can be simplified to a one dimensional problem. If the thermal radiation is neglected, the governing equation is,

$$\frac{\partial\left(\rho c_p T\right)}{\partial t} = k\frac{\partial^2 T}{\partial x^2} + q_0, \tag{1}$$

where ρc_p and k are volume-based specific heat and thermal conductivity of the sample. The solution to this partial differential equation can be got by integral of the Green's function: $G_{X11}(x,t \mid x',\tau) = \frac{2}{L}\sum_{m=1}^{\infty}\exp\left[-m^2\pi^2\alpha(t-\tau)/L^2\right]\sin(m\pi\frac{x}{L})\sin(m\pi\frac{x'}{L})$, and more details can be referred to Guo's work [41]. The boundary conditions are described as $T(x = 0, t) = T(x = L, t) = T_0$. Because the temperature distribution along the wire is expressed as $T(x,t) = T_0 + \frac{\alpha}{k}\int_{\tau=0}^{t}\int_{x'=0}^{L} q_0 G_{X11}dx'd\tau$, so,

$$T(x,t) = T_0 + \frac{4q_0L^2}{k\pi^3}\sum_{m=1}^{\infty}\sin[(2m-1)\pi\frac{x}{L}]\frac{1-\exp\left[-(2m-1)^2\pi^2\alpha t/L^2\right]}{(2m-1)^3}. \tag{2}$$

The average temperature of sample can be integrated and calculated as below,

$$T\left(t\right) = \frac{1}{L}\int_{x=0}^{L} T\left(x,t\right)dx = T_0 + \frac{8q_0L^2}{k\pi^4}\sum_{m=1}^{\infty}\frac{1-exp\left[-\left(2m-1\right)^2\pi^2\alpha t/L^2\right]}{\left(2m-1\right)^4}. \tag{3}$$

The normalized average temperature increase is:

$$T^* = \frac{96}{\pi^4}\sum_{m=1}^{\infty}\frac{1-exp\left[-(2m-1)^2\pi^2\alpha t/L^2\right]}{(2m-1)^4}. \quad (4)$$

The voltage evolution (V_{wire}) recorded by the oscilloscope is directly related to the average temperature change of the sample as

$$V_{wire} = IR_0 + I\eta\frac{8q_0L^2}{k\pi^4}\times T^*, \quad (5)$$

where R_0 is the resistance of the silkworm silk before heating; q_0 is the electrical heating power per unit volume. It is apparent that the measured voltage change is inherently related to the temperature change of the sample. Global fitting of the experimental data (Fig. 2-2) to theoretical solution is performed by trying different trial values of thermal diffusivity and the best fit (least square fitting technique) gives that thermal property of the sample.

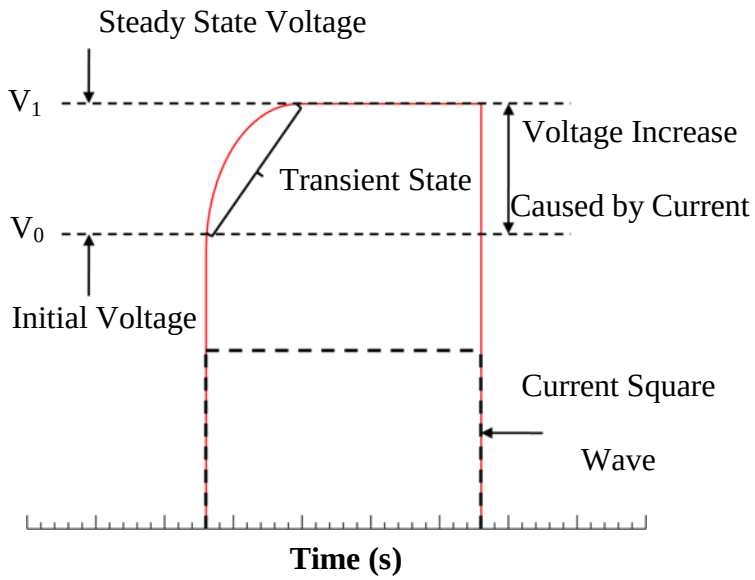

Figure 2-2. Methodology to determine the thermophysical properties based on the experimental *V-t* profile.

2.2 Temperature coefficient of resistance calibration

In equation (3), when *t* (time) goes to infinity, which means the sample reaches at steady state, the average temperature of sample becomes $T_{steady} = T_0 + q_0 L^2 / (12k)$. q_0 is the electrical heating power per unit volume. So the temperature variance $\Delta T = T_{steady} - T_0 = q_0 L^2 / (12k)$ is got. From the experimental result of TET, ΔR is known; from the calibration result, the temperature coefficient of resistance η can be obtained. Then the thermal conductivity is calculated as $k = I^2 RL / (12A\Delta T)$.

The experimental procedure for calibration is very straightforward. After the characterization of the thermal diffusivity of the sample by TET technique, the sample (still suspended on the copper base) is placed on a heater in the vacuum chamber, and after the vacuum chamber is pumped down to about 1 mTorr, the heater is switched on to heat the sample. Thermocouple meter and digital multi-meter are used to record the temperature and resistance of the sample. The temperature coefficient of resistance η can be obtained by curve fitting. For most of the tested materials, when the temperature increment is very small (20-30 degree), the resistance and temperature will have a linear relationship. A typical calibration result for silkworm silk is shown in Fig. 3-1(inset).

2.3 Modification process to derive real thermal properties

For biomaterials, they are nonconductive, so before the characterization, the samples need to be coated with a layer (~nm) of gold film. During the experiment, when the DC current is fed through the sample, the heat flows along the axial direction both in the gold layer and the sample. From the viewpoint of thermal resistance (Fig. 2-3(b)), the gold effect can be easily subtracted. It is apparent that, $1/R_{eff}=1/R+1/R_f$. Here R_{eff}, R, and R_f are the total thermal resistance of the sample coated with gold, the thermal resistance of the sample, and the thermal resistance of the gold layer, respectively.

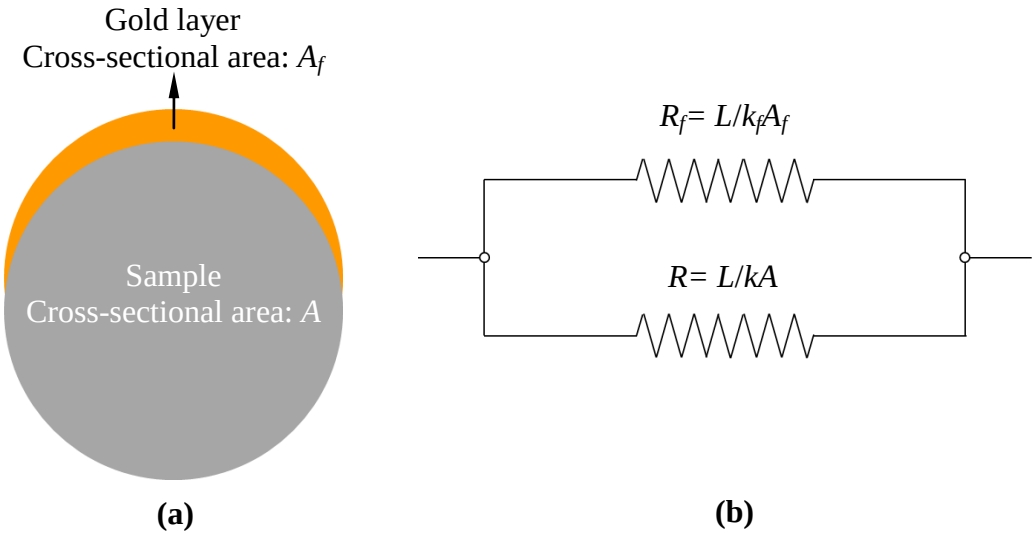

Figure 2-3. (a) Schematic of the cross-section of the sample coated with a layer of gold film. (b) The thermal resistance of the sample and gold layer

So the effective thermal conductivity of the sample coated with gold can be expressed as

$$k_{eff} = \frac{kA + k_f A_f}{A + A_f}, \tag{6}$$

where k_{eff}, k, k_f, A, and A_f are the effective thermal conductivity of the sample coated with gold, the real thermal conductivity of the sample, the real conductivity of the gold layer, the cross-sectional area of the sample, and the cross-sectional area of the gold layer, respectively. Because the thickness of the gold layer is only nm scale, so $A_f << A$, then equation (6) can be simplified as $k_{eff} \cong \frac{kA + k_f A_f}{A}$. Due to the fact that, k_f is very difficult to be tested and it is significantly different from the bulk value, Lorenz number is applied to substitute $k_f A_f$. According to the definition of Lorenz number, $k_f A_f = \frac{L_{Lorenz} TL}{R}$, then the real thermal conductivity of the sample becomes

$$k = k_{eff} - \frac{L_{Lorenz} TL}{RA}. \tag{7}$$

From the references, the Lorenz number is relevant to temperature. When the temperature varies from 0 °C to 100 °C, the Lorenz number for gold varies from 2.35 × 10^{-8} to 2.40 × 10^{-8} W Ω K^{-2} [42]. It is obvious that the change is negligibly small and it is reasonable to treat the Lorenz number as a constant in TET experiment [43]. After testing many groups of spider silk samples, the average value of the Lorenz number for gold on spider silk is about 2.27 × 10^{-8} W Ω K^{-2}, and it is very stable for biomaterials (silkworm silk and human head hair). So this value is used in this work to subtract the gold effect for silkworm silk, spider silk and human head hair samples. If the effective

volume-based specific heat $(\rho c_p)_{eff}$ is known, then the real thermal diffusivity can be obtained:

$$\alpha_s = \alpha_{eff} - \frac{L_{Lorenz} TL}{RA(\rho c_p)_{eff}}. \tag{8}$$

After the real thermal conductivity and thermal diffusivity are calculated, the real volume-based specific heat ρc_p can also be got.

2.4 A new developed technique based on TET

During TET thermal characterization, the surface radiation effect could be significant if the sample has a very large aspect ratio (*L*/*D*, D: sample diameter), especially for samples of low thermal conductivity. Also if the pressure of the vacuum chamber is not very low, the heat transfer to the air will affect the measurement to an ineligible extent. The heat transfer rate of radiation from the sample surface can be expressed as:

$$Q_{rad} = \varepsilon_r \sigma A_s (T^4 - T_0^4) = \varepsilon_r \sigma \pi DL \left(4T_0^3 \theta + 6T_0^2 \theta^2 + 4T_0 \theta^3 + \theta^4 \right), \tag{9}$$

where ε_r is the effective emissivity of the sample, A_s the surface area, T the surface temperature, T_0 the temperature of the environment (vacuum chamber), and $\theta = T\text{-}T_0$. In most cases, $\theta \ll T_0$, then we have:

$$Q_{rad} \approx 4\varepsilon_r \sigma \pi DLT_0^3 \theta. \tag{10}$$

Ignoring the non-consistent heating and convection, which are almost negligible

in our experiment, and converting the surface radiation and gas conduction to body cooling source, the heat transfer governing equation for the sample becomes:

$$\frac{1}{\alpha}\frac{\partial\theta(x,t)}{\partial t}=\frac{\partial^2\theta(x,t)}{\partial x^2}+\frac{I^2R_0}{kLA_c}+\frac{1}{k}\frac{16\varepsilon_r\sigma T_0^{\,3}+4h}{D}\theta\,, \tag{11}$$

where h is the coefficient of gas conduction.

The solution to this partial differential equation can also be got by integral of the Green's function: $G_{X11}(x,t\,|\,x',\tau)=\frac{2}{L}\sum_{m=1}^{\infty}\exp\left[-m^2\pi^2\alpha(t-\tau)/L^2\right]\sin(m\pi\frac{x}{L})\sin(m\pi\frac{x'}{L})$.

The solution to equation (11) is:

$$T(x,t)=T_0+\frac{\pi QL^2}{24}\frac{48}{\pi^4}\sum_{m=1}^{\infty}\frac{1-(-1)^m}{m}\sin\frac{m\pi x}{L}\frac{1-\exp\left[-\left(m^2-f\right)\pi^2(\alpha t/L^2)\right]}{(m^2-f)}. \tag{12}$$

Here f is defined as $(16\varepsilon_r\sigma T_0^{\,3}/D+4h/D)L^2/\pi^2k$. Integrate this equation along the x direction and the average temperature can be obtained:

$$\overline{T(t)}=T_0+\frac{QL^2}{12}\frac{48}{\pi^4}\sum_{m=1}^{\infty}\frac{1-(-1)^m}{m^2}\frac{1-\exp\left[-\left(m^2-f\right)\pi^2(\alpha t/L^2)\right]}{(m^2-f)}. \tag{13}$$

So the normalized average temperature is:

$$T^*=\frac{\overline{T(t)}-T_0}{\overline{T(\infty)}-T_0}=\frac{\sum_{m=1}^{\infty}\left\{\left[1-(-1)^m\right]/m^2\right\}\left\{1-\exp\left[-\left(m^2-f\right)\pi^2(\alpha t/L^2)\right]\right\}/\left(m^2-f\right)}{\sum_{m=1}^{\infty}\left[1-(-1)^m\right]/\left[m^2\left(m^2-f\right)\right]}. \tag{14}$$

After careful numerical and mathematic study, with $\alpha_{eff} = \alpha(1\text{-}f)$, T^* can be approximated as

$$T^* \cong \frac{48}{\pi^4}\sum_{m=1}^{\infty}\frac{1-(-1)^m}{m^2}\frac{1-\exp[-m^2\pi^2\alpha_{eff}t/L^2]}{m^2}. \quad (15)$$

Numeric calculations have been conducted to study the accuracy of the above approximation. It is noticed that, when *f* is less than 0, the maximum absolute difference in the whole transient state is less than 0.014 (shown in Fig. 2-4, Fo stands for the Fourier number, which ranges from 0 to 1). From the equation $\alpha_{eff} = \alpha(1\text{-}f)$, we can get:

$$\alpha_{eff} \cong \alpha + \frac{1}{\rho c_p}\left(\frac{16\varepsilon\sigma T_0^3}{D}+\frac{4h}{D}\right)\frac{L^2}{\pi^2}. \quad (16)$$

This equation demonstrates that measured thermal diffusivity using the TET technique has a linear relation with the effect of radiation and gas conduction. Such theoretical background will be used later to subtract the effect of radiation and gas conduction.

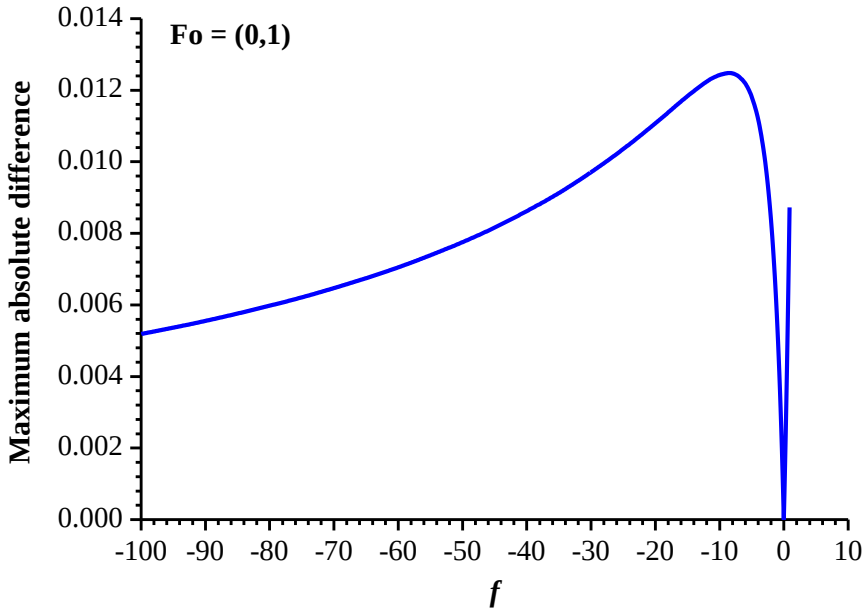

Figure 2-4. The difference between T^* and its approximation using equation (15).

CHAPTER 3. THERMOPHYSICAL PROPERTIES OF SINGLE SILKWORM SILKS AND THE BEHAVIOR UNDER STRETCHING

In this chapter, thermal properties of the original and stretched silkworm silk samples will be investigated by using TET technique and calibration. Section 3.1 introduces the sample preparation process. In section 3.2 the thermal properties of the original and stretched silkworm silks are shown and compared. Three factors combine together to give rise of the remarkable thermal diffusivity increase: alignment improvement of β-sheets blocks, straightening of α-helices and random coils under stretching, and structural transformation from α-helices and random coils to β-sheets by elongation (confirmed by our Raman spectroscopy study).

3.1 Sample preparation

The *Bombyx mori* cocoon is boiled in water at about 100 °C for several minutes. A small wooden rod is used to stir the water, and silks will twist and stick to the rod. The length of the silk got by this hand-reeling method could be as long as 1 m. In order to dry samples, the silk is heated at 140 °C for three hours. Then a silkworm silk sample with a length of 2~3 mm is connected between two copper bases by using silver paste. Because silkworm silk is nonconductive, a gold film of 80 nm is coated on the sample surface to make it electrically conductive.

3.2 Results and discussion

3.2.1 Measurement of thermophysical properties

First of all, we discuss the TET measurement of sample 1 to provide the idea on how the measurement is conducted and analyzed. In the TET technique, the sample is suspended between two copper electrodes. During the experiment, a step DC current is fed through the wire (gold-coated sample) to introduce electrical heating. The temperature increase history of the sample is closely related to the heat transfer along it. The temperature change of the sample will cause a resistance change, which can change the voltage over the wire. So the temperature change of the sample will be monitored by measuring the voltage variation over it. Once the temperature evolution is obtained, the thermal diffusivity of the wire can be obtained by fitting the normalized temperature evolution curve against time. Since silkworm silk is non-conductive, a thin film of gold is coated on its surface to make it conductive. As discussed in Guo's work [39], theoretical fitting of the normalized experimental temperature rise [expressed by equation (4)] is conducted by using different trial values of the thermal diffusivity of the sample. The value giving the best fit of the experimental data is taken as the property of the fiber. Fitting of the experimental data for sample 1 is shown in Fig. 3-1. Its thermal diffusivity is determined at 0.45×10^{-6} m^2 s^{-1}, which includes the influence of the gold coating layer. For comparison, two curves of different thermal diffusivity values are also plotted in Fig. 3-1, one is 1.06α and the other is 0.94α. The fitting uncertainty is about ±6%.

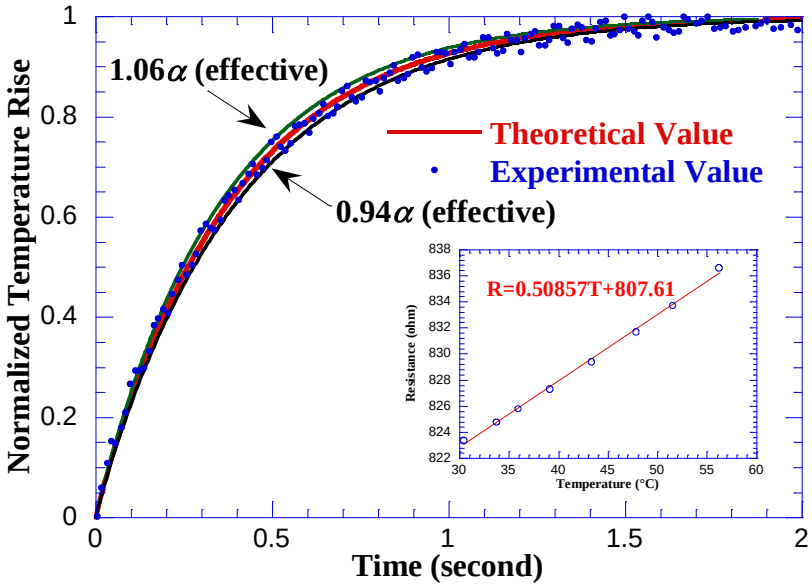

Figure 3-1. Comparison between the theoretical fitting and experimental data for the normalized temperature rise versus time (silkworm silk sample 1) and linear fitting curve of the temperature coefficient of resistance (inset) for the silkworm silk sample 1.

To subtract the effect of gold coating on thermal transport and obtain the real thermal properties, the sample size needs to be determined. A scanning electron microscope (SEM) is used to study the sample size, like length, layer thickness of sericin and the radius of fibroin. Fig. 3-2 shows the SEM images of sample 1. Its length is 2.605 mm, and the diameter of a single fibroin fiber is about 12 μm. Because the silk is composed of two fibrorin fibers and a layer of sericin covering them, a model has been established to calculate the cross-sectional area of the silk based on the SEM images.

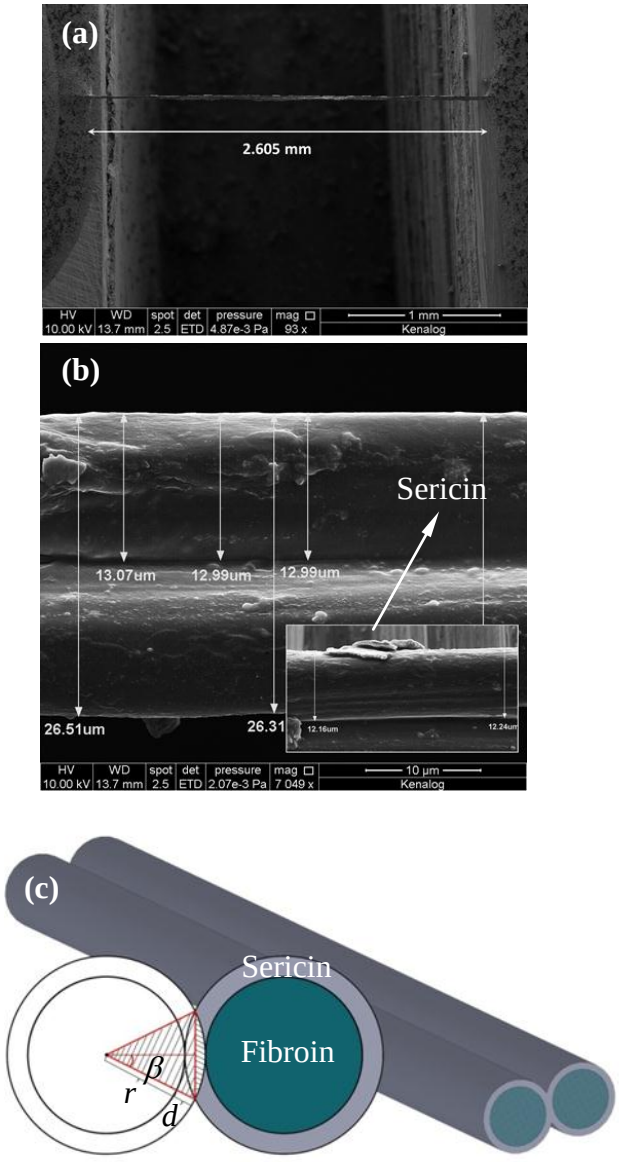

Figure 3-2. SEM pictures, structural model (3D) and cross section (2D) of silkworm silk sample 1. (a) The length of the sample connected between copper bases. (b) The silkworm silk (*Bombyx mori*) composed of two strands of fibroin coated with sericin. The inset in figure (b) shows part of the sericin is dissolved in water during the hand-reeling process. (c) Structural model (3D) and cross section (2D) of silkworm silk. The outside layer (in grey) and inner layer (in dark green) stand for sericin and fibroin, respectively.

The simplified geometry configuration of the silkworm silk is illustrated in Fig. 3-2(c), and we have:

$$\beta = cos^{-1}\left(\frac{r + d/2}{r + d}\right), \tag{17}$$

$$S = (r + d)\left[\pi(r + d)\left(2 - \frac{\beta}{180}\right) - \left(r + \frac{d}{2}\right)sin\beta\right]. \tag{18}$$

Here β stands for the angle showing in Fig. 3-2(c) and S has the same value as A in equation (7) and (8). From Fig. 3-1(b), according to the cross section structure, the value of 26.51, 26.31 and 26.18 μm represents the summation of $4r+3d$. In Fig. 3-1(b) (inset), the small flake on the surface of the silkworm silk should be sericin, which means during the hand-reeling process, some of the sericin may be dissolved in water. It is evaluated the average value of r is 6.10 μm, so the thickness of sericin layer d is 0.64 μm. For sample 5, by using the same method, we obtained d and r, but for sample 2, 3, and 4, it is very difficult to find a part not covered with sericin, so d=0.64 μm is used to calculate r by deducting it from $4r+3d$. The effect of the uncertainty of the thickness of sericin layer on thermal parameters' analysis is almost negligible. The cross-sectional areas of the five measured samples are detailed in Table 3-1. Their fibroin fiber radius is 6.1, 6.08, 6.66, 5.49, and 5.73 μm for sample 1 to 5, respectively, showing a quite uniform silk diameter from sample to sample.

Table 3-1. Details of experimental parameters and results for five silkworm silk samples characterized by using the TET and calibration technique.

Sample	Length (mm)	Cross-sectional area (μm^2)	$\Delta R/\Delta T$ (Ω/K)	ρc_p (real) ($\times 10^6$ J/m^3·K)	α (real) ($\times 10^{-6}$ m^2/s)	k (real) (W/m·K)
1	2.61	284	0.51	1.37	0.39	0.54
2	2.91	282	0.94	1.18	2.03	2.39
3	2.62	333	1.04	3.66	1.78	6.53
4	2.98	234	0.57	1.23	0.90	1.10
5	2.59	277	0.86	1.65	0.83	1.37

The thermal conductivity of the sample is calculated from the calibration procedure and the steady state TET temperature rise. The calibration result of silkworm silk sample 1 is displayed in Fig. 3-1(inset). The temperature–resistance relationship is linear, similar to a metallic conductor. This is because the electrical conduction of the silkworm silk is sustained by the gold coating. The temperature coefficient of resistance, which is 0.51 Ω K^{-1} for sample 1, is obtained by linear fitting of the calibration result [Fig. 3-1(inset)]. During the experiment, a 0.3 mA DC current was fed through this sample, the resistance change is 12.22 Ω and the consequent temperature rise is 24.04 K. The thermal conductivity is derived based on the expression $k=I^2RL/(12A\Delta T)$ as 2.45 W m^{-1} K^{-1}, which includes the influence of the gold coating layer, radiation and rarefied gas conduction in the chamber. A series of experiments have been conducted in our lab to calibrate the effect of radiation and gas conduction using glass fibers. Based on the glass fiber calibration, for sample 1, the effect of radiation and gas conduction on the thermal conductivity is 1.83 W m^{-1} K^{-1}. Therefore the effective thermal conductivity is 0.62 W

m^{-1} K^{-1}. By using $\alpha=k/\rho c_p$, we can obtain ρc_p (effective), then apply equation (7) and (8) to calculate the real thermal diffusivity, conductivity and the volume-based specific heat. The detailed parameters and calculation results for sample 1 is listed in Table 3-2.

Table 3-2. Details of experimental parameters and results for silkworm silk sample 1 characterized by using the TET and calibration technique.

Length (mm)	2.61
Cross-sectional area (μm^2)	284
Resistance (before TET) (Ω)	844.17
Resistance (after TET) (Ω)	856.39
DC current (mA)	0.3
Effective thermal diffusivity ($\times 10^{-6}$ m^2/s)	0.45
Real thermal diffusivity ($\times 10^{-6}$ m^2/s)	0.39
Effective thermal conductivity (W/m·K)	0.62
Real thermal conductivity (W/m·K)	0.54
ρc_p (effective)($\times 10^6$ $J/m^3 \cdot K$)	1.37
ρc_p (real)($\times 10^6$ $J/m^3 \cdot K$)	1.37

3.2.2 Thermal conductivity and diffusivity of relaxed silkworm silk

Details of experimental parameters and results for the five silkworm silk samples are summarized in Table 3-1. The thermal diffusivity and conductivity of silkworm silk vary from 0.39 × 10^{-6}~2.03 × 10^{-6} m^2 s^{-1} and 0.54~6.53 W m^{-1} K^{-1}, respectively. It is apparent that the silkworm silk has a better conductivity compared with other polymers, such as cotton (0.06 W m^{-1} K^{-1}, at 300 K), leather (sole) (0.159 W m^{-1} K^{-1} at 300 K), rubber (vulcanized) (soft, 0.13 W m^{-1} K^{-1}, at 300 K; hard, 0.16 W m^{-1} K^{-1}, at 300 K) [44], PMMA (~0.20 W m^{-1} K^{-1}, at 300 K) [45], and polycarbonate (~0.21 W m^{-1} K^{-1}, at

300 K) [46], but not as good as Kevlar 49 (~30 W m^{-1} K^{-1}, at 300 K). As mentioned above, the thermal conductivity of silk-cloth in the thickness direction is about 0.042 W m^{-1} K^{-1} [13]. It is obvious this result cannot fully reveal the sound thermal transport capability of silkworm silk because of the contact resistance, porosity between the fibers and the difference of the thermal properties in the thickness and axial directions. From Table 3-1, it is noticed that the volume-based specific heat is very consistent except sample 3. Probably this exceptional value is induced by the different structure of this section of the silk or large experiment uncertainty for this sample. The average value of ρc_p for sample 1, 2, 4 and 5 is 1.36×10^6 J m^{-3} K^{-1}. From Table 3-1, the average cross-sectional area of sample 1, 2, 4, and 5 is 269 μm^2. In the next we will use 1.36×10^6 J m^{-3} K^{-1} and 269 μm^2 for thermal parameters analysis under stretching. In this way, there is no need to perform the calibration procedure which is difficult for the experiment under stretching. Actually, the cross-sectional area may change a little in the elongation process, but this parameter is only used for subtracting the effect of gold when calculating the real thermal diffusivity and conductivity by applying equation (7) and (8). After consideration and comparison, the difference caused by this simplification is almost negligible. Take sample 5 as an example, the real cross-sectional area, effective thermal diffusivity and real thermal diffusivity are 277 μm^2, 0.86×10^{-6} m^2 s^{-1} and 0.83×10^{-6} m^2 s^{-1}, respectively. If we assume ρc_p changes from 1.65×10^6 to 1.36×10^6 J m^{-3} K^{-1}, the real thermal diffusivity will change to 0.82×10^{-6} m^2 s^{-1}, which means the 17.6% difference of ρc_p only induces 1.2% change of the real thermal diffusivity. In the same

way, if the cross-sectional area changes to 200 μm^2, the real thermal diffusivity will change to 0.82×10^{-6} m^2 s^{-1}. 27.8% difference of the cross-sectional area also only gives 1.2% change of the real thermal diffusivity. So it is reasonable and convenient to use the average value of ρc_p and the average cross section area, which is 1.36×10^6 J m^{-3} K^{-1} and 269 μm^2, for the thermal parameters analysis of elongated silkworm silk in the next section.

3.2.3 Effect of stretching on thermal conductivity and thermal diffusivity

Seven silkworm silk samples are characterized by using the TET technique twice: one with the original length, and the other one with the elongated length. A spring-control device is used to stretch the silkworm silk. Generally speaking it will take about 10 seconds to do that. And not every sample can be elongated so large and the successful rate is very low for large elongations. Because the gold film on the surface of the sample broke in the elongation process, so the sample was coated with 80 nm of gold film again after stretching to guarantee its conductivity. Considering the variation of thermal diffusivity from sample to sample, the ratio of the thermal diffusivity after stretching to that before stretching for each sample is used to study the elongation effect.

With the purpose of showing the magnificent effect of elongation on thermal properties, the fitting curves of the thermal diffusivity (effective) of the silkworm silk with the original length and elongated length (elongated by 63.76%) are shown in Fig. 3-

3(a). From Fig. 3-3(a) it is noticed that even after elongation, it takes a shorter time for the sample to reach the steady state in the TET measurement. Considering the fact that the thermal diffusivity is proportional to L^2/t_c, where L is the sample length, and t_c the characteristic time to reach steady state, even without fitting we can directly conclude from the raw experimental data that after elongation of 63.76%, the thermal diffusivity should have an increase of at least 168% over that of relaxed silk. Such increase is just magnificent and very exciting. If considering the shorter t_c after stretching, this increase will be even larger and is discussed in the following section. Silkworm silk offers a choice of flexible material for heat transfer. Silkworm silk can be embedded into other low-thermal-conductivity materials to increase the capacity of thermal transport while providing excellent bio-compatible interface. We believe this material should be very promising and may be used in many fields such as flexible electronics and bio-sensors.

The exact experiment results of the seven elongated samples are shown in Table 3-3. α_0 and α_s are the thermal diffusivity (after the subtraction of the gold coating effect) of the same silkworm silk at the original length and elongated length, respectively. Because of the variation of thermal diffusivity of different silkworm silk samples-even obtained from the same cocoon, it makes more sense to use the ratio of thermal diffusivity under different elongation to observe the effect of elongation on the thermal parameters. In Fig. 3-3(b), the blue curve is used to guide eyes to view the data trend. It is clearly shown that the thermal diffusivity is largely improved by elongation initially,

then reaches a peak, and finally drops. Our observation is that when the elongation reaches about 63.8%, the thermal diffusivity, increasing up to 263%, reaches the maximum value/increase.

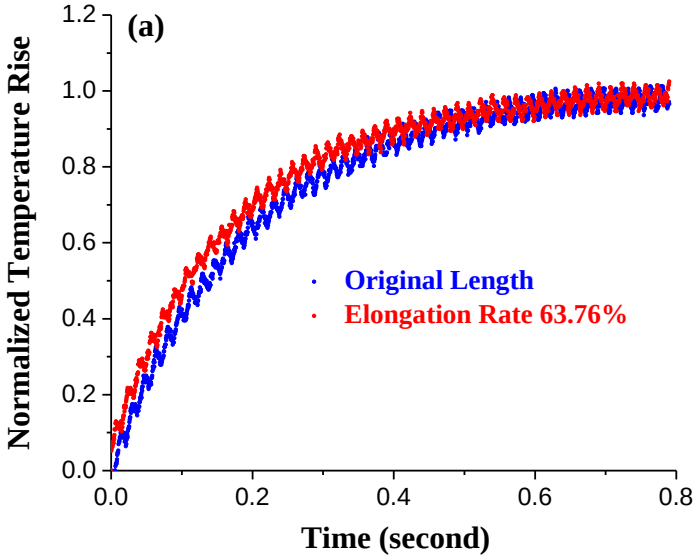

Figure 3-3. (a) The normalized temperature rise for the silkworm silk with the original length and elongated length. (b) The ratio of thermal diffusivity under different elongation. α_0 and α_s are the thermal diffusivity (after subtraction of the effect of the gold) of the same silkworm silk sample with the original length and elongated length, respectively. Here elongation= $(L-L_0)/L_0$, L stands for the length after elongation and L_0 is the original length. The blue curve is used to guide eyes for the trend of data variation.

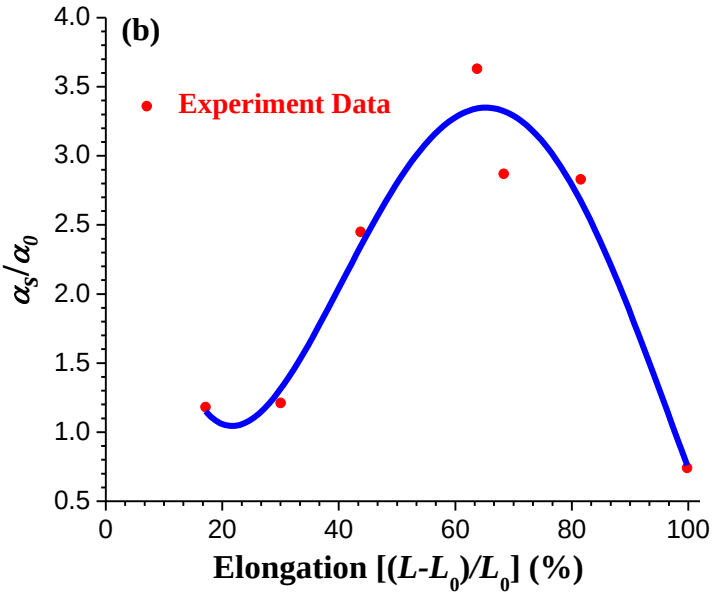

Figure 3-3. Continued.

For silkworm silk, decided by the biological structure and our stretching method, it is difficult to get a draw ratio larger than 2 (elongated by 100%). So the final thermal diffusivity increase is not as much as some polymers, such as single crystal mat polyethylene and gel polyethylene [20]. But under the same stretching ratio (~63.8%), the silkworm silk has a relatively large thermal diffusivity increase. For poly(methyl methacrylate), the thermal conductivity is only increased by less than 10% (at 313 K) under the same stretching [19, 46]. For polycarbonate, the thermal conductivity is increased by about 78% (at 425 K) [46]. Here we introduce a concept of speed of thermal diffusivity increase by stretching as $\zeta = [d(\alpha_e/\alpha_0)/d((L-L_0)/L_0)]$. It can be conveniently used to assess how easy/difficult the thermal transport capability can be improved by stretching. For silkworm silk, ζ is very large (about 4) when the elongation

is from 30 to 50%. When the elongation is ~63.8%, the thermal diffusivity reaches the maximum, and ζ becomes zero. For poly(methyl methacrylate), ζ is only 0.13 (at 313 K) [19]; for polycarbonate, ζ is 1.12 (at 425 K) [46]. For single crystal mat polyethylene, ζ is only 0.16 (at 295 K) [20].

With further elongation, the thermal diffusivity starts to decrease quickly against stretching, indicating break-down of thermal transport path in the silk although the silk does not break yet as seen from outside. For other polymers mentioned above, ζ is always positive, which means under stretching, the thermal diffusivity increase ratio is becoming larger and larger, and no thermal transport path break-down is observed. For the data shown in Table 3-3, after stretching, the thermal diffusivity increases to a higher level. For sample 5, the thermal diffusivity is 9.64×10^{-6} m^2 s^{-1} at the elongation of 68.31%, which is the largest one in the seven samples. Applying the average value of ρc_p, which is 1.36×10^6 J m^{-3} K^{-1}, the thermal conductivity is estimated to be 13.1 W m^{-1} K^{-1}. This value is very high compared with that of polymers mentioned above. It indicates broader applications of silkworm silk in terms of heat dissipation. For other polymers, after stretching, the thermal transport in the direction normal to the stretching direction is reduced [19, 20]. At present, it is still very challenging to measure the thermal diffusivity/conductivity of single silkworm silk in the radial direction. But it is expected the silkworm silk should have the same phenomenon that its thermal transport capability in the radial direction will be reduced significantly by stretching.

Table 3-3. Details of experimental parameters and results for seven elongated silkworm silk samples characterized by using the TET.

Sample	Original Length (mm)	α_0 ($\times 10^{-6}$ m^2 s^{-1})	Elongated Length (mm)	α_s ($\times 10^{-6}$ m^2 s^{-1})	Elongation (%)	α_s/α_0
1	2.35	2.34	2.75	2.77	17.15	1.18
2	1.97	1.64	2.56	1.98	30.05	1.21
3	2.04	1.75	2.94	4.29	43.74	2.45
4	2.41	1.69	3.95	6.13	63.76	3.63
5	2.56	3.36	4.31	9.64	68.31	2.87
6	1.93	1.34	3.50	3.79	81.45	2.83
7	2.13	2.34	4.26	1.74	99.81	0.74

3.2.4 Physics behind the improvement of thermal transport capacity by elongation

A molecular-spring model [11] is established to explore the mystery of the silkworm silk structure [Fig. 3-4(a)] and to explain the elongation effect on the thermal properties in the axial direction. The biological structure of silks can be divided into crystalline (primarily the β-crystallites, which is also a kind of β-sheets structure) and non-crystalline (amorphous) domains, which contain α-helices and random coils [47]. Take the angle of inclination of the β-sheets as θ [shown in Fig. 3-4(b)], and neglect the thermal transportation between strands of β-sheets, from the view point of thermal transport, for the β-sheets blocks we have

$$\frac{\Delta T}{L} kA = \frac{\Delta T}{L\cos\theta} k_{eff} \frac{A}{\cos\theta}. \tag{19}$$

Here ΔT, L, k, k_{eff}, A and θ are temperature difference, the average length of β-

sheets block, average thermal conductivity in the chain direction of β-sheets block, effective thermal conductivity in the axial direction of the silk, the cross-sectional area and the average inclination angel. Then we have $k_{eff} = k\cos^2\theta$. So when θ is 90 degrees, the average thermal conductivity in the chain direction will not contribute to the thermal transport in the axial direction of the silkworm silk. Instead, the weak thermal transport among strands will contribute to the thermal transport in the silk axial direction. In the past, it has been proved that in polymers, the thermal transport along the molecular chain direction is much larger than that in the transverse direction [20]. This is attributed to the fact that vibration (phonons) is easy to transfer along molecular chains rather than from chain to chain.

Similarly, for the spring model of random coils [shown in Fig. 3-4(c)], we have

$$\frac{\Delta T}{L_{tot}} kA = \frac{\Delta T}{L_{eff}} k_{eff} A_{eff} . \tag{20}$$

Here ΔT, L_{tot}, L_{eff}, k, k_{eff}, A and A_{eff} are temperature difference, the average total length of the spring, average effective length of the spring, average thermal conductivity, effective thermal conductivity, the cross-section area and the effective cross-section area. A_{eff} should have a linear relationship with the ratio of L_{tot} and L_{eff}, then we have $k_{eff} = H(L_{eff} / L_{tot})^2$, here H is a constant coefficient.

When the elongation ranges from 0% to about 60%, the effective thermal

conductivity of β-sheets block will be improved as the inclination angle decreases because of stretching [in equation (19)]. This is because under external stretching, the β-sheets crystals will change their orientation to be more aligned along the stretching direction. For random coils, because of the increase of the L_{eff} [in equation (20)] under stretching, the thermal conductivity of this part is also improved a lot. After the peak (when elongation is about 68%) in Fig. 3-3(b), more elongation will cause breakage of the inner bonds, leading to break-down of some random coils. As a result, some β-sheets crystals will lose the external stretching, and their inclination angle θ will become larger again, like that at relaxed state. This will not contribute to the improvement of the thermal conductivity any more. Based on our observation in Fig. 3-3(b), at the elongation of ~64%, the thermal diffusivity starts to decrease, meaning breakdown of the random coils. Since the orientation change of the β-sheets crystal will have very limited contribution to length change (unless the crystal has a large aspect ratio). So we can conclude that the 64% elongation largely comes from the random coils straightening. The breakage of the thermal transport path at 64% elongation leads to one very important conclusion: the length of the random coils under relaxed condition is about 61.1% of their true straight molecular length. When the elongation arrives at about 100%, the silkworm silk will break at any time.

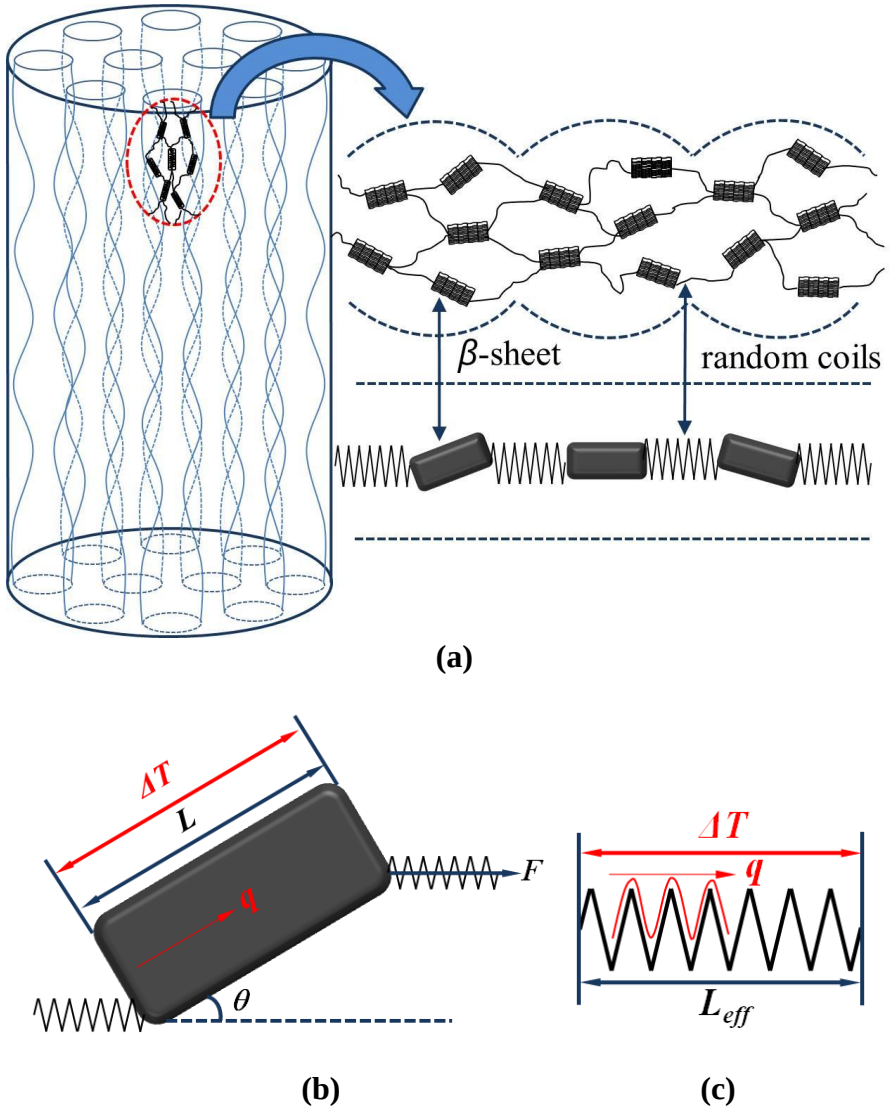

Figure 3-4. (a) The model of the silkworm silk structure. (b) Schematic of thermal transport along the β-sheets crystal. L is the length of the crystal, F the force applied on the silkworm silk during elongation, and θ the angle of inclination. (c) Schematic of thermal transport along the random coils. L_{eff} is the effective length of the spring. q in (b) and (c) stands for the heat flux direction.

3.2.5 Explanation about the improvement of thermal properties after elongation based on Raman spectroscopy

Raman spectra of the silkworm silk under different elongation are studied using a confocal Raman spectrometer (Voyage, BWTek, Inc) coupled with an Olympus BX51 microscope. It employs a 532 nm green laser with 20 mW power as the excitation light source. The beam is focused with 50× objective which gives a laser power about 8 mW on the sample. A sample of silkworm silk is placed over the two legs of a digital caliper and glued with silver paste. The caliper is used to stretch the silk at different elongation until breaking. In order to focus the beam point at almost the same place on the silk after stretching, the caliper is fixed on a precision 3D (XYZ) positioning stage (562 Series ULTRAlign™, Newport) and the stage can offset the original place back to the beam point. It will take about 5 to 30 minutes to focus the laser on the silkworm silk sample, so during this period, the stretched sample will relax (structure stabilizes under the tension). The spectra are collected over the silk at different elongation for an integration period of 20 seconds. No visible silk degradation occurred in the selected experimental conditions. Spectra are corrected for the fluorescence background over the 500-3000 cm^{-1} spectral region by subtracting a polynomial baseline. They are then smoothed by using the Savitzky-Golay method with eight points. Wave number shifts due to experimental conditions of the spectrometer are corrected using the tyrosine band at 1615 cm^{-1} like others did in the literature [48]. There are several main peaks in the Raman plot (Fig. 3-5), like Peak 1 at 1081 cm^{-1} (νCC skeletal stretching, β-sheets and random coil), Peak 2

at 1230 cm^{-1} (amide III, β-sheets and δ CH_2), and Peak 3 at 1665 cm^{-1} (amide I; νC=O in β-sheets) [49]. The relationship between elongation and Raman frequency is obtained and shown in Fig. 3-5(inset).

In Fig. 3-5, spectral changes induced by elongation are plotted. In order to quantitatively show the peaks becoming sharper, full width at half maximum (FWHM) is generated by peak fitting, and the smaller of this value, the sharper of the peak. Under different elongation, from 0% to 60%, peaks (Peak 1 and 2) at 1081 cm^{-1} and 1230 cm^{-1} become sharper. When the elongation is 80%, Peak 1and 2 becomes blunt. It is still very difficult to explain why these two peaks become sharper again when the elongation is over 80%. Because the laser we used in this experiment is not polarized, so the chance that these observations are caused by the improved orientation of the β-sheets with respect to the fiber axis is small. This leads to an important conclusion: the structure transforms from the random coil and α-helices to β-sheets by stretching/elongation from 0% to 60%. This transformation partly contributes to the improvement of thermal diffusivity since the crystal phase is expected to have a higher thermal conductivity than the amorphous phase. This phenomenon is also observed in other polymers under stretching. For single crystal mat polyethylene, the crystallinity can increase from 0.831 to 0.845 when the draw ratio is 6, to 0.932 when the draw ratio is 350. For gel polyethylene, the crystallinity can increase from 0.818 to 0.926 when the draw ratio is 200 [20].

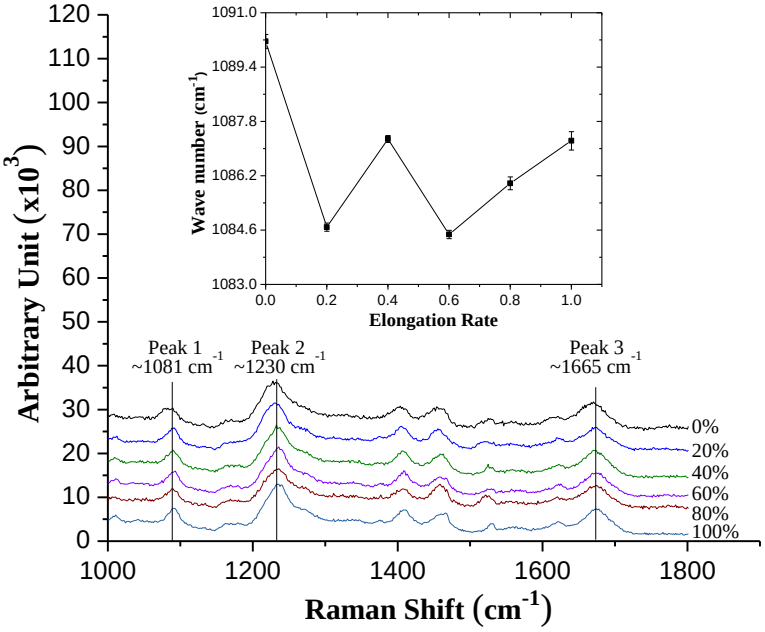

(a)

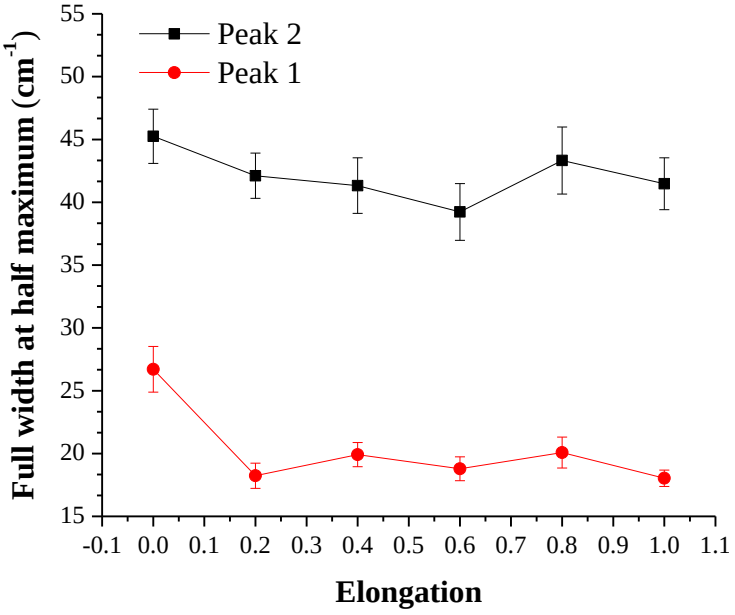

(b)

Figure 3-5. (a) Raman shift changes of fibroin after elongation. The relationship between Raman shift and elongation for Peak 1 is shown in the inset. (b) Full width at half maximum changes of Peak 1 and 2 after elongation.

Generally speaking, for polymer materials, when the strain increases, the stress in the material will increase, and this will cause the decrease of the wave number. At the same time, the thermal conductivity of polymer materials will be negatively affected under strains. In Fig. 3-5(inset), it is apparent that, when the elongation is less than 20%, the Raman frequency is decreasing. The existence of the internal stress will enhance phonon scattering, making the thermal conductivity/diffusivity smaller. However, for silkworm silk, this effect is significantly offset by the alignment effect of the β-sheets crystal, random coil and α-helices. Therefore we only observe a thermal diffusivity increase. Because the hydrogen bonds (its bond strength is only about 8 kJ mol^{-1}) in α-helices and β-sheets are much weaker than the covalent bonds, during the elongation, these bonds may break. By combining Fig. 3-5(inset) and Fig. 3-3(b), it is concluded that, when the elongation varies from 20% to 40%, because of the breakdown of the hydrogen bonds in α-helices, the stress in the sample is partially released, so the wave number increases; when the elongation is about 60%, the wave number reaches its lowest value and the ratio of the thermal diffusivity arrives at its peak; after this point, due to the breakdown of the hydrogen bonds in β-sheets, the Raman frequency begins increasing and the ratio of the thermal diffusivity decreases with the increase of elongation. Our previous speculation based on the observation in Fig. 3-3(b) is that the thermal diffusivity decrease after 64% elongation is because of the breakdown of the β-sheets. Such speculation is confirmed by the observation in Fig. 3-5(inset). After 60% elongation, it is observed the Raman frequency starts to increase. This means the internal

strain/stress has been released partly even the silk is stretched. Such strain/stress release can only be attributed to internal structure break-down. And peaks at 1081 cm^{-1} and 1230 cm^{-1} become blunt when the elongation is 80%, this phenomenon also proves the break-down of the β-sheets. It is noticed that, for Peak 1and 2, they become sharper when the elongation is 100%; for Peak 3, the change of the peak is very small. The mechanism of these phenomena is still unknown. We believe that there are many uncertainties in Raman experiment results reported here. The up-down variation of the Raman peak position could also be caused by unknown experimental uncertainties. So the above argument is not extremely strong. Higher-resolution Raman spectroscopy with highly-controlled environment is needed in future research for studying the structural evolution under stretching.

CHAPTER 4. SILKWORM SILKS, SPIDER SILKS AND HUMAN HEAD HAIR

In Chapter 3, TET is used to characterize the difference of thermal properties between the original and stretched silkworm silks. In order to get more accurate experiment results, a theory is developed to consider the effect of surface radiation and gas conduction during thermal characterization of one-dimensional protein fibers, which is introduced in Chapter 2, Section 2.4. In this chapter, this new technique is applied to test the thermal transport ability of silkworm silks, spider silk, and human head hair (three parts: at the root, in the middle, and at the tip). In Section 4.1, sample preparation process for different samples is introduced. In section 4.2, calculated results from the new technique and calibration are shown to demonstrate the thermal properties of the biomaterials mentioned above.

4.1 Sample preparation: silkworm silk, spider silk and human head hair

The *Bombyx mori* cocoon is boiled in water at about 100 °C for several minutes. A small wooden rod is used to stir the water, and silks will twist and stick to the rod. The length of the silk we get by this hand-reeling method could be as long as 1 m. In order to dry samples, the silk is heated at 140 ˚C for three hours. Then a silkworm silk sample with a length of 2~3 mm is connected between two copper bases by using silver paste. Because silkworm silk is nonconductive, a gold film of 20 nm is coated on the sample surface to make it electrically conductive. Adult female *Latrodectus hesperus* (western

black widow) are collected from Riverside, Riverside County, CA. CO_2 gas is used to anesthetize individual live spiders so they could be secured to the stage of a stereo microscope without injury. Spiders are allowed to recover from the anesthesia before fibers are collected. Major ampullate fibers are manually pulled from the major ampullate spigots on the anterior lateral spinnerets. The pair of major ampullate silk fibers is divided so that a single-stranded fiber could be collected onto a cardboard mount (75 mm × 25 mm with a 20.6 mm hole in the center). The single-strands are affixed to the cards with cyanoacrylate. The human head hair is got from a 30-year old healthy Asian female.

4.2 Results and discussion

4.2.1 Thermal diffusivity characterization

The experimental procedure of TET technique is the same as that introduced in Chapter 3. In the TET technique, the sample is suspended between two copper electrodes. During the experiment, a step dc current is fed through the wire (gold-coated sample) to introduce electrical heating. The temperature increase history of the sample is closely related to the heat transfer along it. The temperature change of the sample will cause a resistance change, which can change the voltage over the wire. So the temperature change of the sample will be monitored by measuring the voltage variation over it. Once the temperature evolution is obtained, the thermal diffusivity of the wire

can be obtained by fitting the normalized temperature evolution curve against time. Fitting of the experimental data for silkworm silk sample 1 is shown in Fig. 4-1(a). Its thermal diffusivity is determined at 5.77×10^{-7} m^2 s^{-1}, which includes the effect of radiation, gas conduction and the influence of the gold coating layer. Repeat this process under different pressures, then a linear relationship between pressure and thermal diffusivity will be revealed (shown in Fig. 4-2). The point where the fitting curve (shown in Fig. 4-2) intersects with the α_{eff}-axis shows the value of α_{eff} when the pressure is 0, which means the gas conduction coefficient in equation (16) is 0. Two silkworm silk samples with different length are tested to get two intersects. By combining these two points, the relationship between α_{eff} and L^2/D can be discovered, then it is very straightforward to calculate the thermal diffusivity of the silkworm silk without the effect of radiation and gas conduction, but with the influence of the gold coating layer.

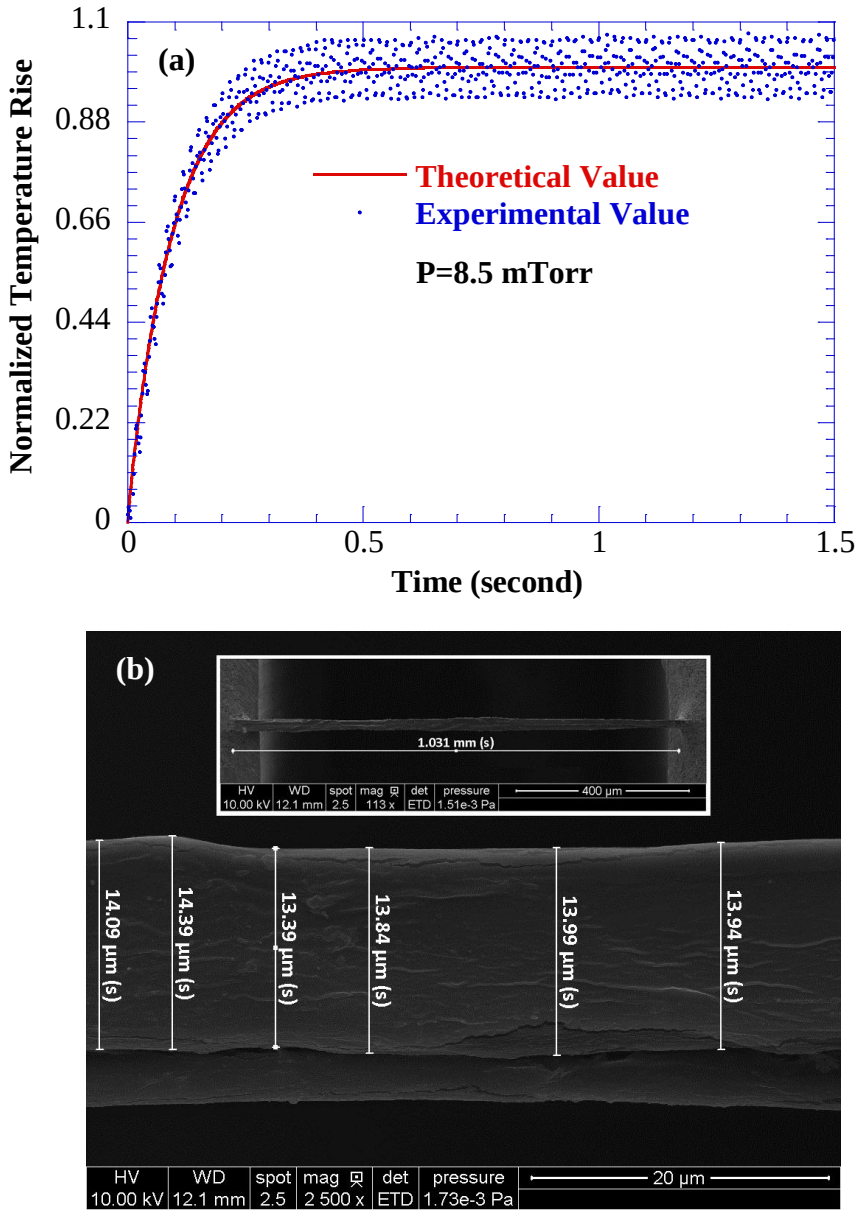

Figure 4-1. (a) Comparison between the theoretical fitting and experimental data for the normalized temperature rise versus time (silkworm silk sample 1) and linear fitting curve of the temperature coefficient of resistance (inset) for the silkworm silk sample 1. (b) SEM images of silkworm silk sample 1, which show the diameter of fibroin (including the layer thickness of sericin) and the sample length (inset).

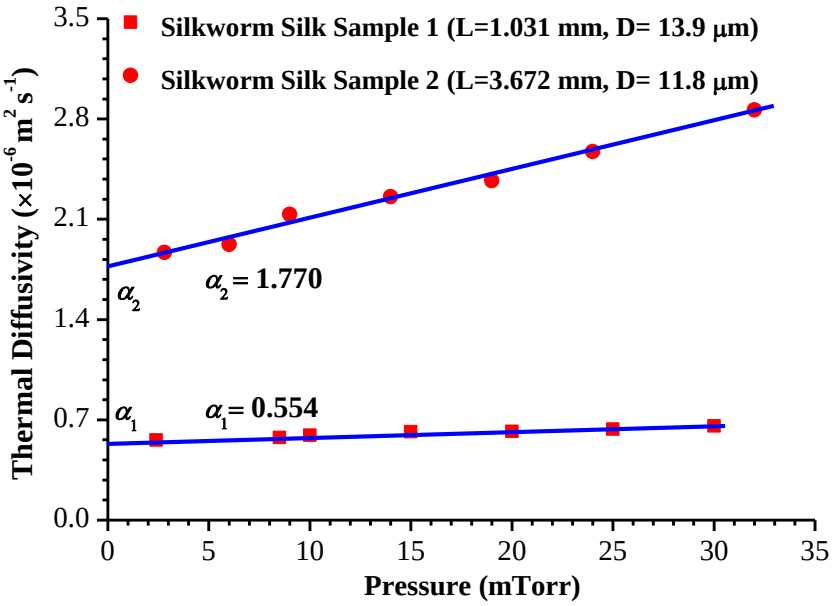

Figure 4-2. The fitting curves of the thermal diffusivity change for the silkworm silk sample 1 and 2 under different pressures.

Equation (8) can be applied to subtract the effect of gold coating on thermal transport and obtain the real thermal properties, because two samples are tested to get the thermal diffusivity of the silkworm silk without the effect of radiation and gas conduction, but with the influence of the gold coating layer, so the average value of *TL*/*RA* can be used for equation (8). The only unknown value is ρc_p-the volume-based specific heat. Here is the procedure to characterize the volume-based specific heat of silkworm silks and a new sample (sample 3) is prepared and tested for this purpose. A scanning electron microscope (SEM) is used to study the sample size, like length and the diameter of fibroin (including the layer thickness of sericin). Its length is 0.568 mm, and

a model is established [27] to get the cross-section area of the sample, which is about 145.26 μm^2. The temperature coefficient of resistance, which is 0.029 $\Omega\ K^{-1}$ for sample 3, is obtained by linear fitting of the calibration result. During the experiment, a 1 mA DC was fed through this sample, the resistance change is 0.33 Ω and the consequent temperature rise is 11.58 K. The effective thermal conductivity is derived based on the expression $k_{eff} = I^2RL/(12A\Delta T)$ as 1.72 W m^{-1} K^{-1}. By using $\alpha = k/\rho c_p$, we can obtain ρc_p, 1.35×10^6 J m^{-3} K^{-1}. For sample 1 and 2, T (the average experiment temperature) can be calculated in this way: $k_{eff} = \alpha_{eff}\, \rho c_p$, $\Delta T = I^2RL/(12Ak_{eff})$. Here α_{eff} is the thermal diffusivity of sample 1 and 2, without the effect of gas conduction, but still having the effect of radiation and gold coating. ΔT is the temperature rise during the experiment. Then plug the values into equation (8), the real thermal diffusivity of silkworm silk can be obtained at last: 3.68×10^{-7} m^2 s^{-1}.

For spider silk and human head hair samples, the procedure to characterize the thermal diffusivity is the same: eliminate the effect of gas conduction firstly and then the effect of radiation, at last, influence of the gold coating layer. The fitting results for spider silk and human head hair are shown in Fig. 4-3 and Fig. 4-4, respectively. The real thermal diffusivity of spider silk and human head hair are 3.53×10^{-7} m^2 s^{-1}, 1.53×10^{-7} m^2 s^{-1} (root), 1.40×10^{-7} m^2 s^{-1} (middle) and 1.49×10^{-7} m^2 s^{-1} (tip), respectively.

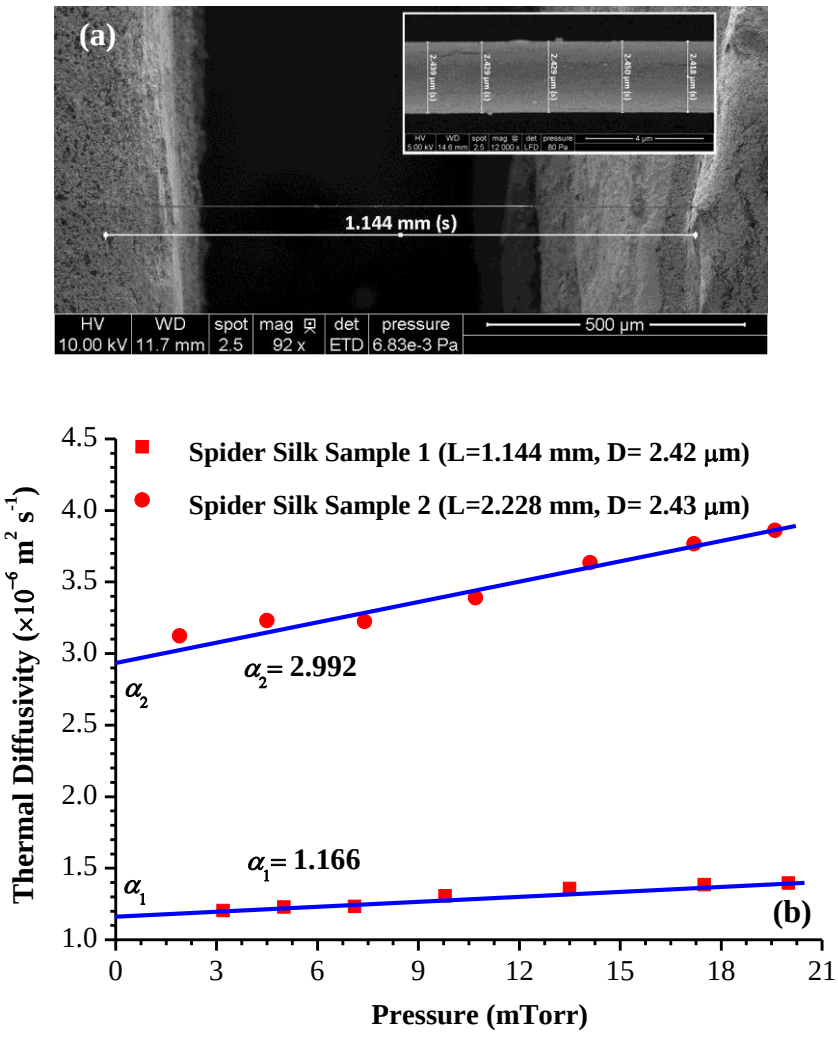

Figure 4-3. (a) The SEM images show the length and diameter of the spider silk sample 1. (b) The fitting curves of the thermal diffusivity change for the spider silk sample 1 and 2 under different pressures.

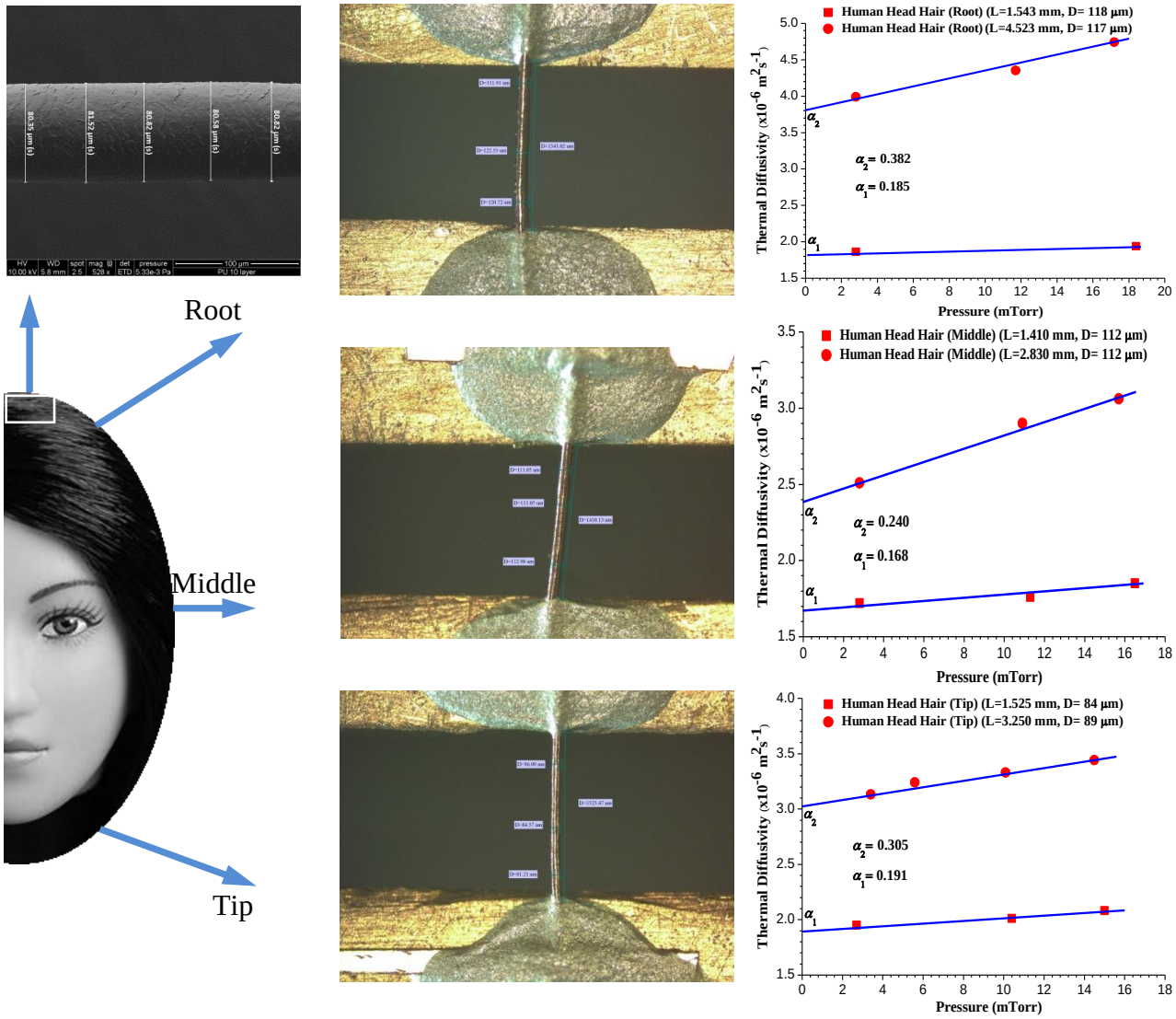

Figure 4-4. The fitting curves of the thermal diffusivity change for human head hair sample 1 and 2 under different pressures are shown on the right, including three parts: root, middle and tip. The microscope images in the middle show the short samples' length. The top left picture is the SEM image of the human head hair.

4.2.2 Comparison of the three materials

For these three kinds of materials, the diameters change from about 2 μm to about 80 μm, and their abilities of thermal transport are very limited. Unlike the spider silk (dragline), whose main function is forming a web frame and supporting the viscid spiral silk to create an orb-web [12], the silkworm silk and human head hair are involved in temperature control for moth pupa and human scalp. For the silkworm silk, cocoon shells produced by silkworm caterpillars are one kind of natural structures and polymeric composite materials which possess excellent mechanical properties. The cocoon not only protects the moth pupa against microbial degradation and desiccation during metamorphosis, but also protects against potential predators [50, 51]. It is very interesting that the elastic modulus, strength and thermo-mechanical parameters all vary along the thickness direction of a cocoon in an apt manner, further enhancing its protection to the pupa from possible attacks from the outside [50]. The thin layer of sericin has many functions: resisting oxidation, antibacterial, ultra-violet resistant, absorbing and releasing moisture easily. The fibroin is well known for its water absorbency, dyeing affinity, thermo tolerances, insulation properties and luster [52]. So it is very reasonable that, this material does not have good heat transfer ability. For human head hair, it is common knowledge that it serves as primary sources of heat insulation and cooling (when sweat evaporates from soaked hair) as well as protection from ultra-violet radiation exposure. It works together with arrector pili muscles to maintain the temperature and protect the scalp. When it is cold, the arrector pili muscles

which are attached to hair follicles will stand up, causing the hair in these follicles to do the same. Then a heat-trapping layer above the epidermis is formed by these hairs (piloerection). When it is hot, the arrector pili muscles will make the hair lie flat on the skin which allows heat to leave. So low thermal transport ability is preferred to fulfill these functions. For the spider silk, the thermal properties are not as high as those reported in the reference [26], three reasons may cause the dramatic difference: 1) The samples we tested for this work are single-stranded major ampullate fibers which are manually pulled from adult female black widows. The samples in the reference are spider silk filaments which are naturally produced by an adult *N. clavipes* female from Florida raised in the laboratory. 2) In the reference, the effect of radiation and gas conduction are not taken into consideration and eliminated. 3) Even if the samples are collected from the same type of spiders, because of the diversity of biomaterials, the thermal properties may also differ from each other noticeably.

4.2.3 Evaluation of thermal conductivity and effective emissivity based on thermal diffusivity

The real thermal conductivity and surface emissivity of the materials can be calculated with the given value of volume-based specific heat (ρc_p), which can be obtained from calibration, noncontact photo-thermal technique [53-55] or testing the density and specific heat separately. For the real thermal conductivity, it is very straightforward that, it can be got by applying $k_{real} = \alpha_{real}\rho c_{p.}$ For effective surface

emissivity, here we take silkworm silk as an example, from the fitting curves in Fig. 4-2(a), the intersects of the two curves are 5.54×10^{-7} m^2 s^{-1} and 17.70×10^{-7} m^2 s^{-1}, multiply them with the value of volume-based specific heat (ρc_p)-here we use 1.35×10^6 J m^{-3} K^{-1}, the effective thermal conductivity (without the effect of gas conduction, but with the influence of radiation and the gold coating layer.) can be characterized:

$$k_{eff} = k_{real} + k_{gold} + \frac{16\varepsilon\sigma T_0^{\,3}}{D}\frac{L^2}{\pi}. \tag{21}$$

Here k_{real} and k_{gold} are the real thermal conductivity, the effect of the gold film on the thermal conductivity, respectively. T_0 is the room temperature, and D is the diameter of the silkworm silk. If we assume that for the same materials, the sum of k_{real} and k_{gold} is the same, then we can have:

$$\varepsilon = \frac{(k_{eff,1} - k_{eff,2})\pi^2}{16\sigma T_0^{\,3}(L_1^2/D_1 - L_2^2/D_2)}. \tag{22}$$

Table 4-1. Details of experimental parameters and results for samples of silkworm silk, spider silk and human head hair (root, middle and tip).

Samples	Silkworm Silk	Spider Silk	Hair (root)	Hair (middle)	Hair (tip)
$\alpha_{real+\,gold}$ ($\times 10^{-7}$ m^2 s^{-1})	4.09	5.09	1.59	1.45	1.57
ρc_p ($\times 10^6$ J m^{-3} K^{-1})	1.35	1.58	1.76	1.76	1.76
α_{real} ($\times 10^{-7}$ m^2 s^{-1})	3.68	3.53	1.53	1.40	1.49
Real thermal conductivity (W m^{-1} K^{-1})	0.50	0.56	0.27	0.25	0.26
Effective emissivity	0.31	0.27	0.32	0.33	0.31

The value of volume-based specific heat (ρc_p) used for silkworm silk and spider silk are obtained by calibration and noncontact photo-thermal technique, respectively. For human head hair, the density is characterized by weighting several hairs and estimating their volume, and the specific heat is tested by DSC (Differential Scanning Calorimetry). The real thermal diffusivity and effective surface emissivity for these three kinds of materials are shown in Table 4-1 in detail.

CHAPTER 5. IMPROVED THERMAL TRANSPORT CAPACITY OF SILKWORM SILKS BY HEAT TREATMENT

In this chapter, it reports on the study of thermal transport in the axial direction of single filaments of silk (*Bombyx mori*) fibroin. The measured thermal diffusivity of the original silk fibroin fiber ranges from 4.05×10^{-7} to 4.65×10^{-7} m^2 s^{-1}. After heat treatment (from about 140 °C to about 220 °C) and subtracting the gold and radiation effect, the real thermal diffusivity of silk fibroin type 1, 2 and 3, increase by 38.12%, 20.72% and 21.35%, respectively. In Section 5.1, three kinds of degumming methods are introduced in detail. In section 5.2, the effect of heat treatment on thermal properties is fully investigated, and a model is proposed to explain the structural change caused by heat treatment.

5.1 Sample preparation

5.1.1 Degumming methods

Three types of silk (*Bombyx mori*) fibroin fibers are prepared by three kinds of degumming methods. The solutions used in this work are neutral soap, strongly alkaline electrolyzed water and Na_2CO_3 solution.

Type 1 fiber: A known weight of clean cocoon shells is added into a 0.2% (W/V) neutral soap solution at a ratio of 1:100 (W/V) and heated at 100 °C for 30 minutes. The

neutral soap solution is removed, replaced with a fresh solution and heated again at 100 °C for 30 minutes. This process is repeated four times. The degummed silk fibroin is washed repeatedly with about 40 °C deionized water. The degummed silk fibroin fibers are also washed repeatedly and air-dried at 105 °C for 2 h.

Type 2 fiber: pH 11.50 strongly alkaline electrolyzed water is used for degumming cocoons. A 2.00 g sample (dry cocoon shells) is mixed with the electrolyzed water (pH 11.50) in a flask at a ratio of 1:40 (W/V). The flask is placed in a boiling water bath (100 °C) for 20 minutes with constant stirring (120 rpm). The degummed silk fibroin fibers from the alkaline electrolyzed water are washed with deionized water and finally air-dried at 105 °C for 2 h.

Type 3 fiber: A known weight of clean cocoon shells is immersed in 0.5% (W/V) Na_2CO_3 at a ratio of 1:20 (W/V) and then heated for 30 minutes at 98 °C. The resulting degummed silk is rinsed repeatedly (the washing water was kept) with 40 °C deionized water then heated again for 30 minutes at 98 °C in 0.5% Na_2CO_3. The degummed silk fibroin is washed repeatedly with about 40 °C deionized water to ensure complete removal of the sericin surrounding the silk fibroin fiber. After washing repeatedly with deionized water, the degummed silk fibroin fibers are air-dried at 105 °C for 2 h and then weighed.

5.1.2 Heat treatment

After being characterized originally, silk fibroin fibers are heated in a bench top muffle furnace (OMEGALUX LMF-A550) at about 140, 160, 180, and 220 °C for 30 minutes, respectively. In order to improve the temperature measurement accuracy, a separate thermal couple has been placed in the chamber to monitor the inside temperature. After heat treatment, the samples are cooled down at room temperature for about 30 minutes before transferred to a vacuum chamber for thermal properties characterization.

5.2 Results and discussion

5.2.1 TET measurement

Here we take silk fibroin fiber sample (type 2) as an example to show the experimental procedure. After being fixed on two copper bases with silver paste, the fiber will be coated with a thin layer of gold (about 40nm) to make it electronically conductive. Then the sample will be placed in a vacuum chamber, which will be pumped down to about 1~3 mTorr. At this pressure, the gas conduction is negligible. A step DC (0.7 mA) is fed through the sample to induce joule heating, and the voltage evolution is recorded by an oscilloscope. For silk fibroin fiber sample (type 2, before heat treatment), fitting of the experimental data is shown in Fig. 5-1(b). Its length is 0.61 mm, and the suspended sample is shown in Fig. 5-1(a). Its thermal diffusivity is determined at

8.24×10^{-7} m^2 s^{-1}, which includes the influence of the gold coating layer and radiation. For comparison, two curves of different thermal diffusivity values are also plotted in Fig. 5-1(b), one is 1.06α and the other is 0.94α. After characterized originally, the sample will be heated in the furnace at a certain temperature (about 140, 160, 180, and 220 °C) for 30 minutes, cooled at the room temperature (about 22 °C) for 30 minutes, and then placed in the vacuum chamber and characterized again. A scanning electron microscope (SEM) is used to check the dimensions (length and diameter) of the sample before and after heat treatment. Details about the experimental conditions and measurement results for silk fibroin fiber sample (type 2) are summarized in Table 5-1. In this table, the effective emissivity and volume based specific heat (ρc_p) are the values we obtained from our former work. According to equation (8) and (16), after subtracting the gold and radiation effect, the real thermal diffusivity of the original silk fibroin fiber sample (type 2) is 4.65×10^{-7} m^2 s^{-1}. Because the simple relationship between the thermal diffusivity and thermal conductivity can be expressed by $k = \alpha \rho c_p$, the real thermal conductivity is determined at 0.63 W m^{-1} K^{-1}.

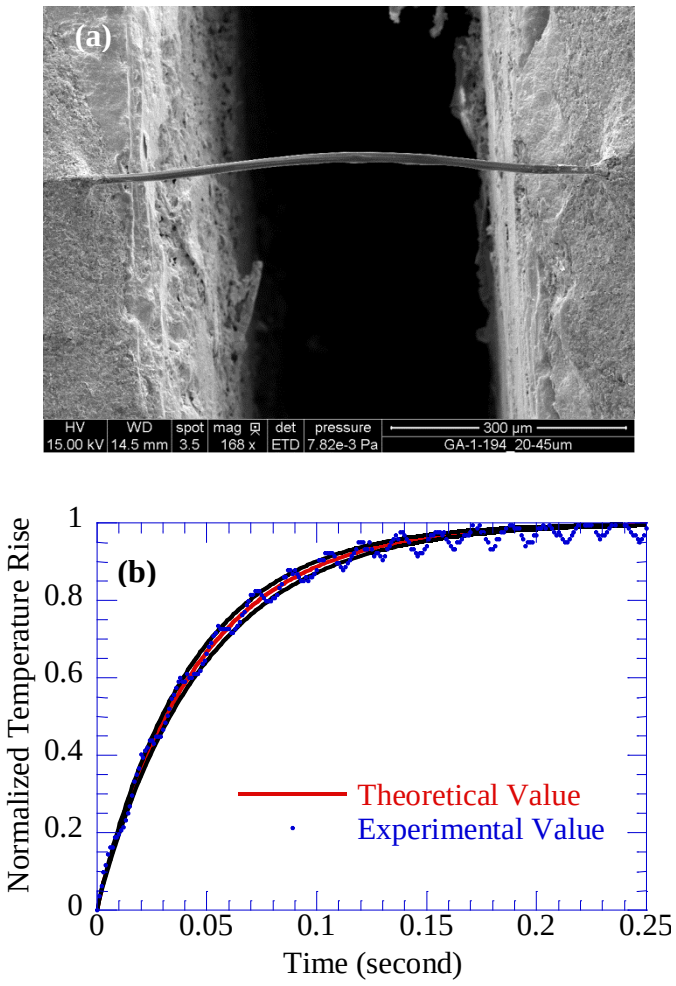

Figure 5-1 (a) A typical SEM image for silk fibroin fiber (Type 2). (b) Comparison between the theoretical fitting and experimental data for the normalized temperature rise versus time (silk fibroin fiber type 2, before heat treatment).

Table 5-1. Details of experimental parameters and results for silk fibroin fiber sample (type 2) characterized by using the TET and calibration technique.

Sample	Type 2
Length (mm)	0.61
Average diameter (μm)	12.02
Cross-sectional area (μm^2)	113
DC current (mA)	0.7
Effective emissivity	0.92
Average resistance before heat treatment (Ω)	87.59
$\alpha_{real+radiation+gold}$ ($\times 10^{-7}$ m^2 s^{-1})	8.24
$\alpha_{real+\ radiation}$ ($\times 10^{-7}$ m^2 s^{-1})	5.15
α_{real} ($\times 10^{-7}$ m^2 s^{-1})	4.65
ρc_p ($\times 10^6$ J m^{-3} K^{-1})	1.35
Real thermal conductivity (W m^{-1} K^{-1})	0.63

5.2.2 Effect of heat treatment

The experimental results of silk fibroin fiber samples type 1, 2 and 3 are shown in Table 5-2 and Fig. 5-2 in detail. Because all of these samples are air-dried at 105 °C for 2 h during initial preparation, so the thermal diffusivity and electrical resistance at 105 °C (the first point of each curve in Fig. 5-2) stand for the properties of the original samples before heat treatment. It is observed that the difference in the original thermal diffusivity among these samples is very small. Before this work, several groups of these three types of original samples have also been characterized, and the average real thermal diffusivity for type 1, 2 and 3 is 3.82 × 10^{-7} m^2 s^{-1}, 3.00 × 10^{-7} m^2 s^{-1} and 3.55 × 10^{-7} m^2 s^{-1}, respectively. The result reported in this work is consistent with that from the

former work considering the sample to sample structure difference. So it is safe to conclude that these three different degumming methods do not result in significant thermal property difference between samples. From Fig. 5-2(a), it is apparent that, after heat treatment, the real thermal diffusivity for type 1, 2 and 3 has been significantly improved by 38.12% (heated at 166.4 °C), 20.72% (heated at 209.8 °C), and 21.35% (heated at 190.6 °C), respectively. The increasing trend of these curves is similar. For type 1 sample, it is very difficult to heat it at higher temperatures (>190 °C) without dramatically increasing the sample resistance to megaohm (electronically nonconductive). For these three types of samples, the saturation point of thermal diffusivity increase is about 166 °C, 140 °C, and 190 °C, after this point, further heat treatment at higher temperatures gives little thermal diffusivity increase.

Table 5-2. Details of experimental results for silk fibroin fiber samples type 1, 2 and 3.

Silk fibroin samples	Temperature (°C)	α_{real} ($\times 10^{-7}$ m^2 s^{-1})	Thermal diffusivity improvement	R_{start} (Ω)	R_{end} (Ω)
Type 1	105.0	4.62	0.00%	141.87	146.00
	143.3	5.60	21.28%	113.30	115.74
	166.4	6.38	38.12%	109.39	111.36
	189.8	5.54	20.06%	124.56	126.90
Type 2	105.0	4.65	0.00%	87.59	89.18
	140.1	5.53	19.08%	85.53	87.00
	160.7	5.60	20.63%	84.81	86.19
	187.2	5.55	19.36%	79.67	80.82
	209.8	5.61	20.72%	69.23	70.27
Type 3	105.0	4.05	0.00%	174.37	179.93
	142.2	4.43	9.26%	161.26	166.25
	166.7	4.39	8.30%	143.44	147.69
	190.6	4.92	21.35%	133.97	137.68
	220.0	4.66	14.93%	118.53	121.74

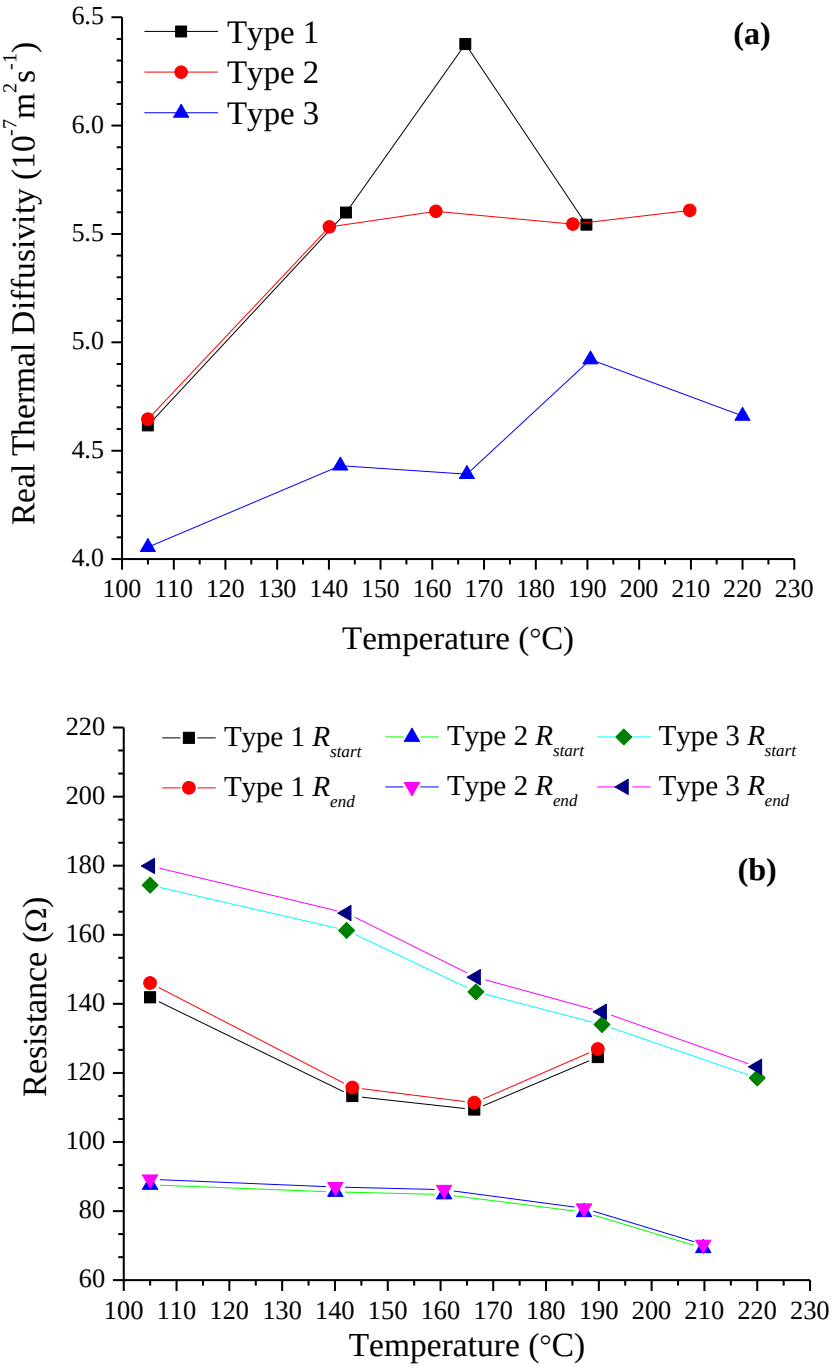

Figure 5-2. (a) The real thermal diffusivity of silk fibroin fiber samples type 1, 2 and 3 before (105 °C) and after heat treatment. (b) The resistance of the samples before (105 °C) and after heat treatment. R_{start} and R_{end} stand for the sample resistance characterized before and after the TET experiment, respectively.

From Fig. 5-2(b), a decreasing trend of the electrical resistance is noticed, which may be contributed by better connections between the gold flakes. According to equation (8), this phenomenon will decrease the *R* value in the denominator, thus increase the value of effective thermal diffusivity (with gold and radiation effect). But after subtracting the gold effect, the effect caused by this trend no longer exists. The results shown in Fig. 5-2(a) already exclude the gold film effect.

5.2.3 Sample structural change by heat treatment

In the past, thermomechanical analysis (TMA) has been applied to monitor the thermal expansion and contraction properties of silks [56]. The thermomechanical analysis curve of *Bombyx mori* silk fiber showed that, from room temperature to 120 °C, the sample experienced a small contraction of about 0.7%. From 120 to 170 °C, the sample length remained almost unchanged. Above 170 °C, it began to extend slightly at a constant rate. The difference of the sample length at room temperature and 220 °C is negligibly small [56]. We used SEM to check the diameter of the samples at the same locations before and after heat treatment (at about 220 °C). Fig. 5-3 shows comparison of the diameter change of these samples, actually several locations are checked for each sample. For type 1 sample, its average diameter increased by 0.44% by heat treatment at 220 °C; for type 2, the average diameter decreased by 1.29%; and for type 3, the average diameter increased by 0.19%. So it is reasonable to use the original diameter and length when calculating the cross-sectional area and subtracting gold and radiation effect during

the above data processing for thermal diffusivity characterization.

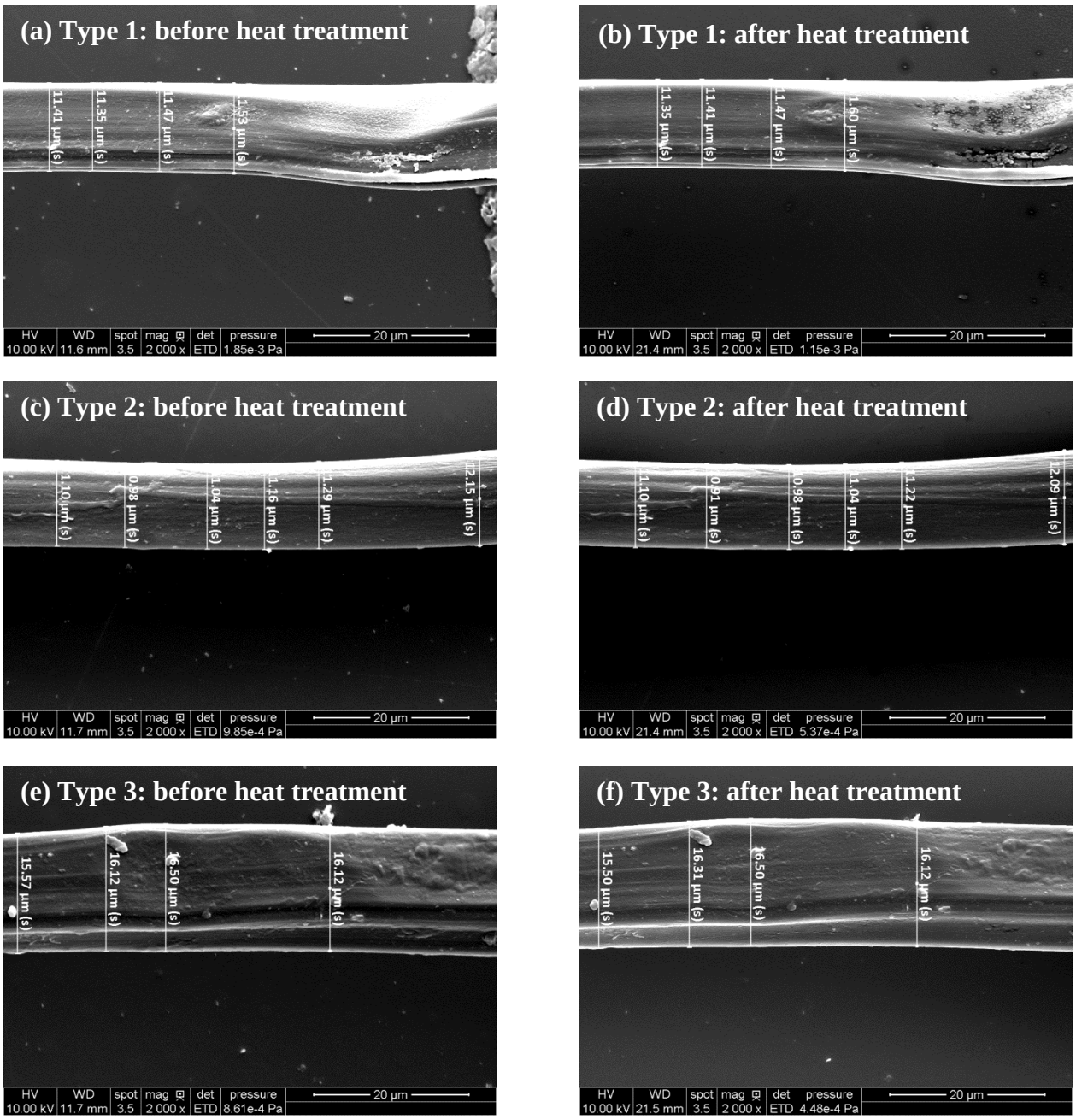

Figure 5-3. (a), (c) and (e) are SEM images of original (before heat treatment) silk fibroin fiber samples, type 1, 2 and 3, respectively. (b), (d) and (f) are SEM images of heat treated (~220 °C) samples, type 1, 2 and 3, respectively.

For RSF films, FTIR and Fourier self-deconvoluted (FSD) curve fitting are usually used to characterize the structural change (from amorphous to crystalline region) and calculate the crystalline degree induced by heat treatment, temperature-controlled water vapor annealing or exposure to chemicals [3, 25, 57]. Because the available FTIR to us has a spot size of 5 mm, too large when compared with the diameter of the single silk fibroin fiber (about 10~20 μm), and the signal is too weak to obtain effective FTIR spectra, so in this work, Raman analysis is performed for the same purpose. Raman spectra of the silk fibroin fibers before (105 °C) and after (147 °C and 179 °C) heat treatment are studied by using a confocal Raman spectrometer (Voyage, BWTek, Inc) coupled with an Olympus BX51 microscope. It employs a 532 nm green laser with 20 mW power as the excitation light source. The beam is focused with 50× objective which gives a laser power about 8 mW on the sample. During the analysis, it is observed that the Raman intensity of samples heated at 179 °C is very small, thus cannot be effectively used to compare with that of original samples and samples heated at 147 °C. The situation becomes even worse after the samples heated above 179 °C, and the laser can easily burn them. There are several main peaks in the Raman plot (Fig. 5-4) which relate to β-sheets: Peak 1, at 1081 cm^{-1} (νCC skeletal stretching, β-sheet, random coil); Peak 2, at 1230 cm^{-1} (amide III, β-sheet, δ CH_2 tw); and Peak 3, at 1665 cm^{-1} (amide I, νC=O in β-sheets) [49]. In order to quantitatively show the peaks becoming sharper, full width at half maximum (FWHM) is generated by peak fitting, and the smaller of this value, the sharper of the peak. The difference of FWHM for Peak 1, 2 and 3 (type 1, 2 and 3)

before and after heat treatment are shown in Fig. 5-4(inset). It is apparent that, after the heat treatment at 147 °C, these peaks become slightly sharper, which means the β-sheets (crystallinity degree) may be increased or the orientation of the β-sheets with respect to the fiber axis is improved. Due to the fact that the laser used in this experiment is not polarized, so the chance for the latter mechanism is small.

A research group has done a full test (thermomechanical analysis, dynamic mechanical properties, x-ray diffraction and the refractive indices) of the structural changes of silk (*Bombyx mori* and *Antheraea pernyi*) fibers induced by heat treatment [56]. Though based on the x-ray diffraction curves, the crystalline structure of *Bombyx mori* silk fibers stayed unchanged after heat treatment. The isotropic refractive index (n_{iso}), which is related to the crystallinity of the fiber, did show a linear increase in the temperature range examined. A structure model, which is composed of amorphous regions, crystalline regions and laterally ordered regions, has been proposed to explain the structural changes induced by heat treatment. It is concluded in that work that, due to the close packing of the more adjacent laterally ordered regions, the number and size of the crystalline regions of *Bombyx mori* silk fibroin was increased by heat treatment.

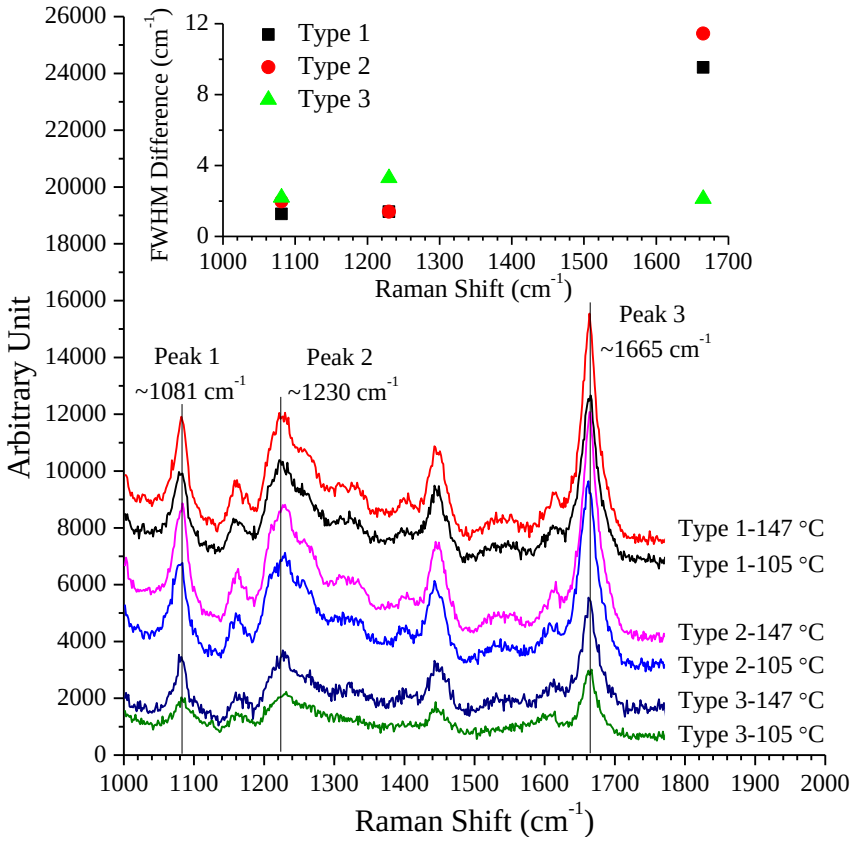

Figure 5-4. Raman analysis of silk fibroin fiber samples type 1, 2 and 3 before (105 °C) and after (147 °C) heat treatment. The inset shows the difference of full width at half maximum of Peak 1, 2 and 3 before and after heat treatment.

For silk fibroin fibers naturally produced by silkworms, the crystallinity is approximately as high as 62%-65% [58]. For RSF films of *Bombyx mori*, the crystallinity can be increased to 43% by heat treatment at 214 °C, to 56% by exposing in methanol at room temperature for four days, and to 57.8-59.6% by water vapor annealing at 90-100 °C [3, 25]. It is apparent that, naturally produced fibroin fibers have the highest crystallinity. It is highly possible that, even being treated by various methods, the transformation from amorphous to crystalline structure though exists, but such

transition should be very limited. Some references [3, 59, 60] also point out that, the x-ray diffraction analysis tends to be inaccurate at low crystalline fraction, because that many of the formed crystals are too small or imperfect to measurably contribute to the overall coherent scattering in the x-ray diffraction pattern. Taking all these factors into consideration, that explains why the x-ray diffraction did not detect the crystalline structural change of *Bombyx mori* silk fibers after heat treatment, and why in our Raman analysis, the peaks at 1081, 1230 and 1665 cm^{-1} becomes only slightly sharper. It is well known that the crystal phase is expected to have a higher thermal conductivity than the amorphous one [61-64]. Based on the truth that how difficult it is to characterize the tiny structural change precisely and how dramatically the thermal property changes by even small structural change, it leads to an important point that, thermal property characterization can be used to reflect the overall structural change of the protein fibers under various treatments.

Silkworm silk has a good ability of absorbing water. For RSF film, it generally contains 5-10% (w/w) water without humidity treatment [65, 66]. For silk fiber naturally produced by silk works, it takes about 5% water [67]. When the temperature is lower than 100 °C, which is the atmospheric boiling point of water, water may contribute significantly to the fluctuation of the thermal properties of different samples. For our silk fibroin fiber samples, the last step in sample preparation is air-drying them at 105 °C for 2 h. Under this circumstance, the water effect on the thermal properties should be

removed. In order to have a sense of the water effect on the samples, we characterized three groups of type 1 samples (no heat treatment) using the TET technique, then soaked them in water for 30 minutes, air-dried them at room temperature for 30 minutes, and characterized them again. For type 1 sample 1, the effective thermal diffusivity (includes gold and radiation effect) decreased by 9.31%; for type 1 sample 2, increased by 10.97%; for type 1 sample 3, increased by 1.25%. The changes of the effective thermal diffusivity do not have any trend, and could be induced by the gold film structure change by soaking and drying. The small water concentration change in the sample has little effect on the thermal diffusivity. Therefore we conclude that the thermal diffusivity increase observed in Fig. 5-2 is induced by the structure change/crystallinity increase rather than loss of the little water concentration in the silk.

CHAPTER 6. CONCLUSION AND FUTURE WORK

6.1 Conclusion of thermal properties of micro/nanoscale materials

6.1.1 Original and stretched silkworm silks

The thermal diffusivity of silkworm silk without elongation varied from 0.39 $\times 10^{-6}$ to 2.03 $\times$ 10^{-6} m^2 s^{-1}, and the thermal conductivity was in a range of 0.54~6.53 W m^{-1} K^{-1}. Compared with other polymers, the thermal conductivity of silkworm silks is very high. The thermal diffusivity of silkworm silk was largely improved when elongated to about 60%. Under 63.8% elongation, the thermal diffusivity was observed to have an increase of 263%, meaning the thermal diffusivity of silkworm silk under elongation is more than three times that at the original length. So it is easy to achieve large manipulation of thermal transportation. For one of the samples studied (Sample 5), after elongation of 68.31%, its thermal conductivity was estimated to be 13.1 W m^{-1} K^{-1}. The decrease of the inclination angle of the β-sheets blocks, the increase of the effective length of spring model of random coils, and the transformation from the random coil to β-sheets by elongation contributed to the improvement of thermal diffusivity. When the silkworm silk was elongated beyond 64%, more and more inner bonds were broke, which caused decrease of thermal diffusivity. Our Raman spectroscopy study of the silkworm silk under elongation also confirmed this speculation. After 60% elongation, the Raman frequency started to increase. This means the internal strain/stress has been

released even the silk is stretched. Such strain/stress release can only be attributed to internal structure break-down.

6.1.2 Thermal properties characterization of three kinds of biomaterials by using the new technique

A linear relationship between the effective thermal diffusivity and pressure-which has an effect on the effective thermal diffusivity in the form of gas conduction-is discovered and proved. Just by testing two samples of the same material with different length, the effect of radiation and gas conduction can be eliminated. Given the value of volume-based specific heat (ρc_p), the real thermal diffusivity, real thermal conductivity and effective surface emissivity of the materials can be calculated. This work reports on the much more accurate characterization of thermal transport in the axial direction of single silkworm silk, spider silk and human head hair (three parts: at the root, in the middle, and at the tip). The measured real thermal diffusivity of silkworm silk, spider silk and human head hair is 3.68×10^{-7} m^2 s^{-1}, 3.53×10^{-7} m^2 s^{-1}, 1.53×10^{-7} m^2 s^{-1} (at the root), 1.40×10^{-7} m^2 s^{-1} (in the middle) and 1.49×10^{-7} m^2 s^{-1} (at the tip), respectively. The functional requirements may decide that the thermal transport ability of silkworm silk and human head hair is not very good.

6.1.3 Improved thermal properties of silk fibroin fibers induced by heat treatment

The measured thermal diffusivity of the original silk fibroin fiber ranges from 4.05×10^{-7} to 4.65×10^{-7} m^2 s^{-1}. After heat treatment (from about 140 °C to about 220 °C) and subtracting the gold and radiation effect, the real thermal diffusivity of silk fibroin type 1, 2 and 3, increase by as high as 38.12%, 20.72% and 21.35%, respectively. The sample diameter change is almost negligible which is proved by checking the diameter of the sample at the same place before and after heat treatment by SEM, which is consistent with the thermomechanical analysis curve from the literature. Raman analysis was performed on the original and heat-treated (heated at about 147 °C and 179 °C) samples. After the heat treatment at 147 °C, the peaks at 1081, 1230 and 1665 cm^{-1} become slightly sharper, and this is probably caused by the structural transformation from amorphous region to crystalline region. According to the literature, a model composed of amorphous regions, crystalline regions and laterally ordered regions is proposed to explain the structural changes induced by heat treatment. Due to the close packing of the more adjacent laterally ordered regions, the number and size of the crystalline regions of *Bombyx mori* silk fibroin increased by heat treatment. Thus the thermal properties of the samples are significantly improved. Because of the sensitivity of the thermal property change caused by the structural change of the sample, in the future, the characterization of the thermal property may be developed and used as a standard method to reflect the overall structural change (crystalline degree or β-sheets

content) of the protein fibers, if an accurate correlation between these two parameters can be determined.

6.2 Future work

After characterizing the silk fibers naturally produced by silkworms, no matter it is original or degummed, how to improve or change the thermal properties becomes next step. In this work, the effect of stretching and heat treatment on the thermal properties is investigated. From the literature, most of the thermal analysis of silk fibroins is focused on RSF films [3, 65, 67, 68], not the native silks (like our samples) naturally produced by silkworms. For RSF films, there are various ways to induce structural changes (from amorphous region to crystalline region). For temperature-controlled water vapor annealing, the β-sheets crystallinity can increase from 14% (when the water vapor annealing temperature is 4 °C) to 57.8-59.6% (when the water vapor annealing temperature is 90-100 °C) [25]. Exposing to chemicals, such as ethanol and methanol, can also affect the crystallization of β-sheets [3, 25, 57]. These studies have already shown the structure changes of the samples, but never characterized the thermal diffusivity, so in the future: (1) the effect of temperature-controlled water vapor annealing and exposing to chemicals on the thermal properties of native silks naturally produced by silkworms needs to be tested; (2) the thermal property changes of the RSF films induced by heat treatment, temperature-controlled water vapor annealing and exposing to chemicals need to be characterized.

For RSF films, FTIR and Fourier self-deconvoluted (FSD) curve fitting are widely used to test the structural change. The advantage of this method is that the crystalline degree induced by various treatments can be conveniently calculated. Some researchers even found a correlationship between the heat capacity increment and β-sheets fraction in *Bombyx mori* silk. Because of the sensitivity of the thermal property change caused by the structural change of the sample, in the future, the characterization of the thermal property may be developed and used as a standard method to reflect the overall structural change (crystalline degree or β-sheets fraction) of the protein fibers, if an accurate correlation between these two parameters can be determined.

REFERENCES

1. Asakura, T., et al., *Comparative structure analysis of tyrosine and valine residues in unprocessed silk fibroin (silk I) and in the processed silk fiber (silk II) from Bombyx mori using solid-state C-13, N-15, and H-2 NMR.* Biochemistry, 2002. **41**(13): p. 4415-4424.
2. Altman, G.H., et al., *Silk-based biomaterials.* Biomaterials, 2003. **24**(3): p. 401-416.
3. Hu, X., D. Kaplan, and P. Cebe, *Determining beta-sheet crystallinity in fibrous proteins by thermal analysis and infrared spectroscopy.* Macromolecules, 2006. **39**(18): p. 6161-6170.
4. Foo, C.W.P. and D.L. Kaplan, *Genetic engineering of fibrous proteins: spider dragline silk and collagen.* Advanced Drug Delivery Reviews, 2002. **54**(8): p. 1131-1143.
5. Demura, M., T. Asakura, and T. Kuroo, *Immobilization of Biocatalysts with Bombyx-Mori Silk Fibroin by Several Kinds of Physical Treatment and Its Application to Glucose Sensors.* Biosensors, 1989. **4**(6): p. 361-372.
6. Zhou, C.Z., et al., *Fine organization of Bombyx mori fibroin heavy chain gene.* Nucleic Acids Research, 2000. **28**(12): p. 2413-2419.
7. Yamaguchi, K., et al., *Primary Structure of the Silk Fibroin Light Chain Determined by Cdna Sequencing and Peptide Analysis.* Journal of Molecular Biology, 1989. **210**(1): p. 127-139.

8. Inoue, S., et al., *Silk fibroin of Bombyx mori is secreted, assembling a high molecular mass elementary unit consisting of H-chain, L-chain, and P25, with a 6 : 6 : 1 molar ratio.* Journal of Biological Chemistry, 2000. **275**(51): p. 40517-40528.

9. Kaplan, D., et al., *Silk - Biology, Structure, Properties, and Genetics.* Silk Polymers, 1994. **544**: p. 2-16.

10. Sirichaisit, J., et al., *Analysis of structure/property relationships in silkworm (Bombyx mori) and spider dragline (Nephila edulis) silks using Raman Spectroscopy.* Biomacromolecules, 2003. **4**(2): p. 387-394.

11. Wu, X., et al., *Unraveled mechanism in silk engineering: Fast reeling induced silk toughening.* Applied Physics Letters, 2009. **95**(9): p. 093703.

12. Lim, V.I. and S.V. Steinberg, *A Novel Structural Model for Silk Fibroin - Alpha-L-Alpha-R-Beta-Structure.* Febs Letters, 1981. **131**(2): p. 203-207.

13. Rood, E.S., *Thermal conductivity of some wearing materials.* Physical Review, 1921. **18**(5): p. 356-361.

14. Choy, C.L., *Thermal-Conductivity of Polymers.* Polymer, 1977. **18**(10): p. 984-1004.

15. Lee, G.W., et al., *Enhanced thermal conductivity of polymer composites filled with hybrid filler.* Composites Part a-Applied Science and Manufacturing, 2006. **37**(5): p. 727-734.

16. Tavman, I.H., *Thermal and mechanical properties of aluminum powder-filled high-density polyethylene composites.* Journal of Applied Polymer Science, 1996. **62**(12): p. 2161-2167.

17. Hellwege, K.H., W. Knappe, and J. Hennig, *Anisotropie Der Warmeausdehnung Und Warmeleitung Ind Einachsig Verstreckten Amorphen Hochpolymeren.* Acta Veterinaria Academiae Scientiarum Hungaricae, 1963. **13**(4): p. 121-127.

18. Hands, D., *The Effect of Biaxial Orientation on the Thermal-Conductivity of Vulcanized and Un-Vulcanized Rubber.* Rubber Chemistry and Technology, 1980. **53**(1): p. 80-87.

19. Washo, B.D. and D. Hansen, *Heat Conduction in Linear Amorphous High Polymers - Orientation Anisotropy.* Journal of Applied Physics, 1969. **40**(6): p. 2423-2427.

20. Choy, C.L., et al., *Elastic Modulus and Thermal Conductivity of Ultradrawn Polyethylene.* Journal of Polymer Science Part B: Polymer Physics, 1999. **37**(23): p. 3359-3367.

21. Washo, B.D. and D. Hansen, *Heat Conduction in Linear Amorphous High Polymers - Orientation Anisotropy.* Journal of Applied Physics, 1969. **40**(6): p. 2423.

22. Vandenbrule, B.H.A.A., *A Network Theory for the Thermal-Conductivity of an Amorphous Polymeric Material.* Rheologica Acta, 1989. **28**(4): p. 257-266.

23. Uemura, O., et al., *Thermally Induced Crystallization of Amorphous Ge0.4se0.6.* Journal of Non-Crystalline Solids, 1990. **117**: p. 219-221.

24. Exarhos, G.J. and N.J. Hess, *Spectroscopic Measurements of Stress-Relaxation during Thermally Induced Crystallization of Amorphous Titania Films.* Thin Solid Films, 1992. **220**(1-2): p. 254-260.

25. Hu, X., et al., *Regulation of Silk Material Structure by Temperature-Controlled Water Vapor Annealing.* Biomacromolecules, 2011. **12**(5): p. 1686-1696.

26. Huang, X.P., G.Q. Liu, and X.W. Wang, *New Secrets of Spider Silk: Exceptionally High Thermal Conductivity and Its Abnormal Change under Stretching.* Advanced Materials, 2012. **24**(11): p. 1482-1486.

27. Liu, G., et al., *Thermal transport in single silkworm silks and the behavior under stretching.* Soft Matter, 2012. **8**(38): p. 9792-9799.

28. Lu, L., W. Yi, and D.L. Zhang, *3 omega method for specific heat and thermal conductivity measurements.* Review of Scientific Instruments, 2001. **72**(7): p. 2996-3003.

29. Choi, T.Y., et al., *Measurement of the thermal conductivity of individual carbon nanotubes by the four-point three-omega method.* Nano Letters, 2006. **6**(8): p. 1589-1593.

30. Hou, J.B., et al., *Thermal characterization of single-wall carbon nanotube bundles using the self-heating 3 omega technique.* Journal of Applied Physics, 2006. **100**(12): p. 124314-124319.

31. Kim, P., et al., *Thermal transport measurements of individual multiwalled nanotubes.* Physical Review Letters, 2001. **87**(21): p. 215502.

32. Kim, P., et al., *Mesoscopic thermal transport and energy dissipation in carbon nanotubes.* Physica B-Condensed Matter, 2002. **323**(1-4): p. 67-70.

33. Shi, L., et al., *Measuring thermal and thermoelectric properties of one-dimensional nanostructures using a microfabricated device.* Journal of Heat Transfer-Transactions of the Asme, 2003. **125**(6): p. 881-888.

34. Li, D.Y., et al., *Thermal conductivity of individual silicon nanowires.* Applied Physics Letters, 2003. **83**(14): p. 2934-2936.

35. Shi, L., et al., *Thermal conductivities of individual tin dioxide nanobelts.* Applied Physics Letters, 2004. **84**(14): p. 2638-2640.

36. Hou, J.B., X.W. Wang, and J.Q. Guo, *Thermal characterization of micro/nanoscale conductive and non-conductive wires based on optical heating and electrical thermal sensing.* Journal of Physics D-Applied Physics, 2006. **39**(15): p. 3362-3370.

37. Feng, X.H. and X.W. Wang, *Thermophysical properties of free-standing micrometer-thick Poly (3-hexylthiophene) films.* Thin Solid Films, 2011. **519**(16): p. 5700-5705.

38. Feng, X., et al., *Thermo-physical properties of thin films composed of anatase TiO_2 nanofibers.* Acta Materialia, 2011. **59**(5): p. 1934-1944.

39. Guo, J.Q., X.W. Wang, and T. Wang, *Thermal characterization of microscale conductive and nonconductive wires using transient electrothermal technique.* Journal of Applied Physics, 2007. **101**(6): p. 063537.

40. Guo, J.Q., et al., *Transient thermal characterization of micro/submicroscale polyacrylonitrile wires.* Applied Physics a-Materials Science & Processing, 2007. **89**(1): p. 153-156.

41. Wang, X.W., J.Q. Guo, and T. Wang, *Thermal characterization of microscale conductive and nonconductive wires using transient electrothermal technique.* Journal of Applied Physics, 2007. **101**(6).

42. Kumar, G.S., G. Prasad, and R.O. Pohl, *Experimental Determinations of the Lorenz Number.* Journal of Materials Science, 1993. **28**(16): p. 4261-4272.

43. R. W. Powell, R.P.T.a.M.J.W., *Thermal Conductivities and Electrical Resistivities of the Platinum Metals.* Platinum Metals Rev., 1962. **6**: p. 138-143.

44. Incropera, F.P., D.P. DeWitt, and T.L. Bergman, *Fundamentals of heat and mass transfer*. 2007, p. 939-40, Hoboken, NJ: John Wiley.

45. Eiermann, K. and K.H. Hellwege, *Thermal Conductivity of High Polymers from -180 Degrees C to 90 Degrees C.* Journal of Polymer Science Part B: Polymer Physics, 1962. **57**(165): p. 99-106.

46. Choy, C.L., W.P. Leung, and Y.K. Ng, *Thermal-Diffusivity of Polymer-Films by the Flash Radiometry Method.* Journal of Polymer Science Part B-Polymer Physics, 1987. **25**(9): p. 1779-1799.

47. Simmons, A.H., C.A. Michal, and L.W. Jelinski, *Molecular orientation and two-component nature of the crystalline fraction of spider dragline silk.* Science, 1996. **271**(5245): p. 84-87.

48. Lefevre, T., M.E. Rousseau, and M. Pezolet, *Protein secondary structure and orientation in silk as revealed by Raman spectromicroscopy.* Biophysical Journal, 2007. **92**(8): p. 2885-2895.

49. Colomban, P., et al., *Nanomechanics of single silkworm and spider fibres: a Raman and micro-mechanical in situ study of the conformation change with stress.* Journal of Raman Spectroscopy, 2008. **39**(12): p. 1749-1764.

50. Zhao, H.P., et al., *Mechanical properties of silkworm cocoons.* Polymer, 2005. **46**(21): p. 9192-9201.

51. Kirshboim, S. and J.S. Ishay, *Silk produced by hornets: thermophotovoltaic properties - a review.* Comparative Biochemistry and Physiology a-Molecular & Integrative Physiology, 2000. **127**(1): p. 1-20.

52. Mondal, M., K. Trivedy, and S.N. Kumar, *The silk proteins, sericin and fibroin in silkworm, Bombyx mori Linn., - a review.* Caspian Journal of Environmental Sciences, 2007. **5**(2): p. 63-76.

53. Hu, H.P., X.W. Wang, and X.F. Xu, *Generalized theory of the photoacoustic effect in a multilayer material.* Journal of Applied Physics, 1999. **86**(7): p. 3953-3958.

54. Wang, X.W., H.P. Hu, and X.F. Xu, *Photo-acoustic measurement of thermal conductivity of thin films and bulk materials.* Journal of Heat Transfer-Transactions of the Asme, 2001. **123**(1): p. 138-144.

55. Wang, T., et al., *Effect of zirconium(IV) propoxide concentration on the thermophysical properties of hybrid organic-inorganic films.* Journal of Applied Physics, 2008. **104**(1).

56. Tsukada, M., et al., *Structural-Changes of Silk Fibers Induced by Heat-Treatment.* Journal of Applied Polymer Science, 1992. **46**(11): p. 1945-1953.

57. Lu, Q., et al., *Water-insoluble silk films with silk I structure.* Acta Biomaterialia, 2010. **6**(4): p. 1380-1387.

58. Warwicker, J.O., *Comparative Studies of Fibroins .2. Crystal Structures of Various Fibroins.* Journal of Molecular Biology, 1960. **2**(6): p. 350-&.

59. Asakura, T., et al., *Conformation Characterization of Bombyx-Mori Silk Fibroin in the Solid-State by High-Frequency C-13 Cross Polarization Magic Angle Spinning Nmr, X-Ray-Diffraction, and Infrared-Spectroscopy.* Macromolecules, 1985. **18**(10): p. 1841-1845.

60. Um, I.C., et al., *Structural characteristics and properties of the regenerated silk fibroin prepared from formic acid.* International Journal of Biological Macromolecules, 2001. **29**(2): p. 91-97.

61. Yamasaki, M., S. Kagao, and Y. Kawamura, *Thermal diffusivity and conductivity of Zr55Al10Ni5Cu30 bulk metallic glass.* Scripta Materialia, 2005. **53**(1): p. 63-67.

62. Huang, Z.X., et al., *Thermal conductivity of amorphous and crystalline thin films by molecular dynamics simulation.* Physica B-Condensed Matter, 2009. **404**(12-13): p. 1790-1793.

63. Nath, P. and K.L. Chopra, *Thermal-Conductivity of Amorphous and Crystalline Ge and Gete Films.* Physical Review B, 1974. **10**(8): p. 3412-3418.

64. Shukla, N.C., et al., *Thermal conductivity and interface thermal conductance of amorphous and crystalline Zr47Cu31Al13Ni9 alloys with a Y2O3 coating.* Applied Physics Letters, 2009. **94**(8).

65. Hu, X., D. Kaplan, and P. Cebe, *Effect of water on the thermal properties of silk fibroin.* Thermochimica Acta, 2007. **461**(1-2): p. 137-144.

66. Motta, A., L. Fambri, and C. Migliaresi, *Regenerated silk fibroin films: Thermal and dynamic mechanical analysis.* Macromolecular Chemistry and Physics, 2002. **203**(10-11): p. 1658-1665.

67. Guan, J., D. Porter, and F. Vollrath, *Thermally Induced Changes in Dynamic Mechanical Properties of Native Silks.* Biomacromolecules, 2013. **14**(3): p. 930-937.

68. Hu, X., D. Kaplan, and P. Cebe, *Dynamic protein-water relationships during beta-sheet formation.* Macromolecules, 2008. **41**(11): p. 3939-3948.